Speed, Shape and Chase-Escape: Stochastic Evolution in Models of Statistical Physics

A Thesis

submitted to
Indian Institute of Science Education and Research Pune
in partial fulfillment of the requirements for the
BS-MS Dual Degree Programme

by

Aanjaneya Kumar

Indian Institute of Science Education and Research Pune
Dr. Homi Bhabha Road,
Pashan, Pune 411008, INDIA.

April, 2019

Supervisor: Prof. Deepak Dhar

Certificate

This is to certify that this dissertation entitled *Speed, Shape and Chase-Escape:* Stochastic Evolutions in Models of Statistical Physics towards the partial fulfillment of the BS-MS dual degree programme at the Indian Institute of Science Education and Research, Pune represents study/work carried out by Aanjaneya Kumar at Indian Institute of Science Education and Research under my supervision during the academic year 2018-2019.

Deepak Dhar

Prof. Deepak Dhar

Committee:

Prof. Deepak Dhar

Dr. M. S. Santhanam

"Here's to the ones who dream, foolish as they may seem.
Here's to the hearts that ache, here's to the mess we make."

Declaration

I hereby declare that the matter embodied in the report entitled *Speed, Shape and Chase-Escape*: Stochastic Evolution in Models of Statistical Physics are the results of the work carried out by me at the Department of Physics, Indian Institute of Science Education and Research, Pune, under the supervision of Prof. Deepak Dhar and the same has not been submitted elsewhere for any other degree.

Aanjaneya Kumar

Acknowledgments

I would like to thank my supervisor Prof. Deepak Dhar for his encouragement, guidance and patience. I also owe a special thanks to Dr. MS Santhanam who patiently guided me throughout my time at IISER Pune and to Dr. Tridib Sadhu with whom I had many useful and fruitful discussions. This work wouldn't have been possible if it wasn't for them and the constant support of my family and friends (canine or otherwise). My time at IISER Pune has taught me a lot and I will always deeply cherish every moment spent here and every memory created here.

Abstract

In this thesis, we study simple stochastic models that show rich and interesting behavior. The plan of the thesis is as follows: after a brief introduction and overview of the work in Chapter 1, Chapter 2 begins with a discussion on the simplest stochastic interacting particle system − *the exclusion process*. After briefly motivating the process, we will describe a two-species exclusion problem that shows a remarkable, counter-intuitive feature, called the *TASEP Speed Process*. Our aim in this chapter will be to provide a simple approximate description for this phenomena using what we here call the *effective medium approach*. After addressing the issue of the TASEP Speed Process, we will extend our approach to different variations of the multi-species exclusion process. Following the discussing in this chapter on a system of stochastically interacting particle system, in Chapter 3, we will discuss the stochastic evolution of a surface, taking the example of the *Eden Model*. We start with an small exposition of the process and its variants following which, we will motivate the question of finding upper bounds to the shape of growing clusters using examples from day-to-day life. In this chapter, we will obtain upper bounds of increasing accuracy by using the independent branching process and its variants. In Chapter 4, we will move on to the study of the stochastic evolution of a model with two interacting surfaces, called *Chase-Escape*. This process, defined as a prey-predator model, shows a very interesting feature that the prey can survive even when it can run only half as fast as the predators. After studying the critical properties of this process, we will compare the dynamics of the front of Chase-Escape process with the Eden front. Our analysis of this problem will be partly inspired by our analysis of the Eden process in the previous chapter. In Chapter 5, we will present a summary of all our results and will outline future directions.

Contents

Chapter 1

Introduction

We begin our journey into *Stochastic Evolution in Models of Statistical Physics* by very briefly introducing ourselves to the fascinating world of non-equilibrium statistical physics and laying out a plan for the rest of the thesis. Here, we will define the three exciting stochastic processes, all of which have their origins in problems in Biology, that will form the main focus of the thesis and will motivate the purpose of studying each of them.

Statistical Physics is a branch of science that deals with systems consisting of many particles interacting with each other where we attempt to better understand the phenomena that emerge out of these interactions, many of which are not accessible through reductionist treatments. Systems that are in thermal equilibrium obey the laws of Equilibrium Statistical Physics − a subject whose tools are mature and well developed. However, unlike its equilibrium counterpart, Non-Equilibrium Statistical Physics does not have an overarching formalism. But in the last three decades, this field has seen a substantial amount of progress. A significant portion of this recent progress has come through the use of a *kinetic* approach. The idea of this approach is to study simple stochastic models specified by dynamical rules which capture the essence of the real process that we are trying to describe. Once the model and its dynamical rules are established, the next step is to analyze these simple models, and through this analysis, uncover what more can the model tell us about the real process. To do so, we develop an array of tools and methods that help us understand the process better. And with this kinetic approach as the guiding principle, we begin our study of *Stochastic Evolution in Models of Statistical Physics.*

The plan of the thesis is as follows: Chapter 2 begins with a general discussion on the simplest stochastic interacting particle system − the *exclusion process*. After briefly motivating the process and discussing what is known, we will describe a two-species exclusion problem that shows a remarkable, counter-intuitive feature, called the *TASEP Speed Process*. More precisely, we will discuss the approximate phenomenological description of the motion of a single second-class particle in a two-species totally asymmetric simple exclusion process (TASEP) on a 1D lattice. Initially, the second class particle is located at the origin and to its left, all sites are occupied with first class particles while to its right, all sites are vacant. Ferrari and Kipnis [14] proved that in any particular realization, the average velocity of the second class particle tends to a constant, but this mean value has a wide variation in different histories. We will discuss this phenomenon called TASEP Speed Process, in an approximate effective medium description, in which the second class particle moves in a random background of the space-time dependent average density of the first class particles. We do this in three different approximations of increasing accuracy, treating the motion of the second-class particle first as a simple biased random walk in a continuum Langevin equation, then as a biased Markovian random walk with space and time dependent jump rates, and finally as a Non-Markovian biased walk with a non-exponential distribution of waiting times between jumps. We will show that when the displacement at time T is x_0, the conditional expectation of displacement, at time zT ($z > 1$) is zx_0, and the variance of the displacement only varies as $z(z-1)T$. We will extend this approach to describe the trajectories of a tagged particle in the case of a *finite* lattice, where there are L classes of particles on an L-site line, initially placed in the order of increasing class number. Lastly, we will discuss a variant of the problem in which the exchanges between adjacent particles happened at rates proportional to the difference in their labels. After addressing the issue of the TASEP Speed Process, we will extend our approach to different variations of the multi-species exclusion process.

In Chapter 3, we will discuss the stochastic evolution of a surface, taking the example of the *Eden Model*. We start with an small exposition of the process and its variants following which, we will motivate the question of finding upper bounds to the shape of growing clusters using examples from day-to-day life. We will then discuss three approximations to determine the Eden cluster shape on a d-dimensional hypercubical lattice, in terms of region visited up to time t by an independent branching process (IBP) on the d-dimensional hypercubical lattice and two modifications to it − one in which each cell independently gives rise to daughter cells at neighbouring sites except along the bond that connects it to its mother cell

and the other, in which we iteratively evolve the system and in each iteration, impose the condition at any non-empty site, no more cells can be added due to the descendants of the cells present at that site. All three of these will provide upper bounds to the region reached in the original infection process, and will become asymptotically exact in the large-d limit. Even in $d = 2$, we will show that the simplest IBP approximation is rather good.

In Chapter 4, we will move on to the study of the stochastic evolution of a model with two competing surfaces, called *Chase-Escape* and will study its critical properties. This process, defined as a prey-predator model on the $2-$D square lattice, shows an intriguing survival-extinction phase transition for the prey. The prey can co-exist with predators even it is moving at a speed significantly lesser than that of the of the predators. While this is not unexpected, the issue gets very interesting when it is noted that the estimated critical value of the rate of spreading of prey $p_c = 0.5 \pm 0.01$, which is the critical value of the classic bond percolation on the $2-$D square lattice. We will study Chase Escape Percolation on the $2-$D square lattice and determine its critical value using numerical simulations to be $p_c = 0.4943 \pm 0.001$. This provides strong evidence against the idea that the Chase-Escape percolation might be the bond percolation in disguise. We will also establish that the critical behaviour of this process in different directions is not different by finding that $p_c = 0.4943 \pm 0.001$ in the diagonal direction as well. Apart from this phase transition, the Chase-Escape front also undergoes a *depinning* transition. For $p_c < p < 1$, the center of mass of the red and blue fronts coincide as a function of time and the two fronts move together in a *pinned* way. Interestingly, we will show that the speed of the Chase-Escape front is smaller than the speed of the Eden front for the same value of p. Using simulations, we will provide a possible mechanism for this counter-intuitive phenomena. Finally, we will provide a lower bound to the cluster size distribution for $p < p_c$.

We will conclude in Chapter 5 by providing a brief summary of our results and outline future directions for research that arise as a consequence of the results obtained in this thesis.

In the problems considered for this project, I have tried my best to first understand the process to the best of my abilities and then to provide simple descriptions to the rich phenomena that is observed in these processes. Approximate descriptions that capture the phenomenology of the process are going to be a recurring theme in the coming chapters of the thesis. Another theme that will be common in our analysis will be going beyond the simple description by making better approximations, by incorporating more elements of the

processes that we are trying to model, and hence providing models that, with increasing accuracy, describe aspects of the real process.

Chapter 2

TASEP Speed Process: An Effective Medium Approach

Advantage begets further advantage − this effect, often called the Matthew effect, is observed in various forms in day-to-day life, most commonly in social and economic aspects. But can such an effect be seen in systems where the evolution is completely memory-less? The answer is *yes.* In this chapter, we will study a Markov process in which, the dynamics of a special particle at late times is heavily determined by its dynamics at early times. We will provide a simple description of this phenomena and using simple models, improve upon the current understanding of this phenomena.

2.1 Introduction

There has been a lot of interest in understanding exclusion processes on a line as the simplest model of stochastic evolution in systems of interacting particles [1]. In the simple symmetric exclusion process on a 1−D lattice, we start with an initial condition where particles occupy some lattice sites with the constraint that each lattice site can at most accommodate one particle. In the continuous time version of this process, the time evolution of the system is given by the rule that each particle hops to an empty nearest neighbour site with rate 1. Many exact results are known for this simple exclusion process on a line [5]. Several variants of the exclusion process have been studied including multi-species exclusion processes and

the partially and totally asymmetric exclusion processes (ASEP and TASEP) [1, 5 − 8]. These have found several interdisciplinary applications and are good models of many physical systems, such as traffic on highways [2], transport in narrow channels [3] and motion of motor proteins on microtubules [4].

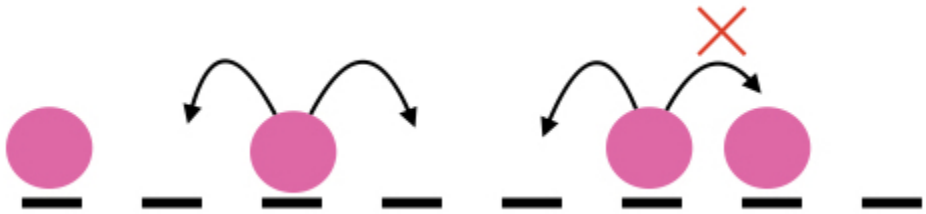

Figure 2.1: A schematic representing an exclusion process. Particles can only hop to empty nearest neighbours.

If we want to study the trajectory of individual particles in an assembly of interacting particles, one often adopts a self-consistent mean-field kind of approximation, in which the motion of the particle occurs in an effective field provided by the others. The best known example being Brownian motion [9, 10], that was first studied to describe the motion of pollen grains in a liquid. In this case, the molecules present in the liquid provide a random fluctuating force, that leads to a diffusive motion of the pollen grains. The strength of the random force is determined by some average macroscopic properties of the liquid like the effective viscosity and temperature. Other examples of self-consistent treatments include the Hartree-Fock theory of electronic structure of atoms [11, 12], and the motion of ions in plasmas in the Vlasov approximation [13].

In this chapter, we will discuss this general approach, called the *effective medium* approach here, in the specific setting of a two-species totally asymmetric exclusion process. We will consider a system of hard-core particles on a 1-dimensional lattice, with two classes of particles. We will consider the evolution from the special initial condition, where there is only one second class particle at the origin, and all sites sites to the left are occupied by first class particles, and all sites to the right of the origin are vacant. The dynamics follows continuous-time Markovian evolution where each first class particle exchanges position with a second-class particle or vacancy to its right with rate 1. The second class particle can jump to the left, if forced by a first class particle moving from its left, or jump one space to an empty site on its right, with rate 1.

For this problem, Ferrari and Kipnis made a rather surprising observation [14]. In their

own words, "a second class particle initially added at the origin chooses randomly one of the characteristics with the uniform law on the directions and then moves at constant speed along the chosen one." This is a remarkable property as the system undergoes Markovian evolution, and has no memory. It happens, because if the second-class particle initially, by chance, gets a large positive displacement, in subsequent times it encounters a smaller density of other particles, and hence also moves faster at later times. This is an example of persistence, where time average of one evolution history is very different from ensemble average over all histories of evolution.

While the authors proved this result, they did not discuss how big are the fluctuations in the velocity, and how they decrease with time. In this chapter, we will describe this process in a simple Langevin description [15], that also allows us to estimate how the fluctuations in the average speed decrease with time.

We will show that, when the displacement of the second class particle at time T is x_0, the conditional expectation of displacement, at time zT ($z > 1$) is zx_0, and the variance of the displacement only varies as $z(z-1)T$. Thus the fluctuations, for fixed z, increase as $\sqrt{T}$. Equivalently, we find that if v^* is the asymptotic value of velocity of the second class particle, for large z, $(v^* - x_0/T)$ has a typical spread of $\frac{1}{\sqrt{T}}$ which goes to 0 as T increases.

The plan of this chapter is as follows: in Section 2.2, we define the model precisely. In section 2.3, we discuss the description of the trajectory of the second-class particle in a Langevin equation description. We use this to determine the variance of the particle position at time zT, given the position at time T. In Section 2.4, we discuss different approximations of increasing accuracy describing the trajectory as a biased random walk. In section 2.5, we then use this approach to study the mean trajectories in a more complicated problem called the Oriented Swap Process. Section 2.6 contains a summary and concluding remarks that includes the description of an interesting open problem.

2.2 Definition of the Process

We consider a two species TASEP with initial conditions such that a single second class particle is located at the origin of the lattice. To the left of the second class particle, each lattice site is occupied by a first class particle and to its right, each site is vacant. We will

denote a first class particle by 1, a second class particle by 2 and a vacant site (hole) by 0. The allowed nearest neighbour transitions in this process are:

$$10 \xrightarrow{rate\,\Gamma} 01$$

$$20 \xrightarrow{rate\,\Gamma} 02$$

$$12 \xrightarrow{rate\,\Gamma} 21$$

We set $\Gamma = 1$.

We wish to understand the dynamics of the second class particle in this process. Ferrari and Kipnis proved [14] that the position of the second class particle $X(t)$ at time t follows:

$$\lim_{t\to\infty} \frac{X(t)}{t} = U$$

where U is a uniform random variable on $[-1, 1]$.

We will call the process in which the velocity of the second class particle tends to a random number distributed uniformly between $[-1, 1]$ as *TASEP Speed Process* (TSP) and will provide a simple explanation of this remarkable phenomena. The name TSP earlier has been used in the study of joint distribution of the velocities of different particles in a multi-species version of this process [16].

2.3 Langevin Description

We aim to understand the motion of the second class particle, when all the sites to its left are occupied by first class particles and all sites to its right are vacant, using a simple approximation by breaking this problem into two steps:

1. We first discuss how the mean density $\rho(x, t)$ of first class particles evolves in space

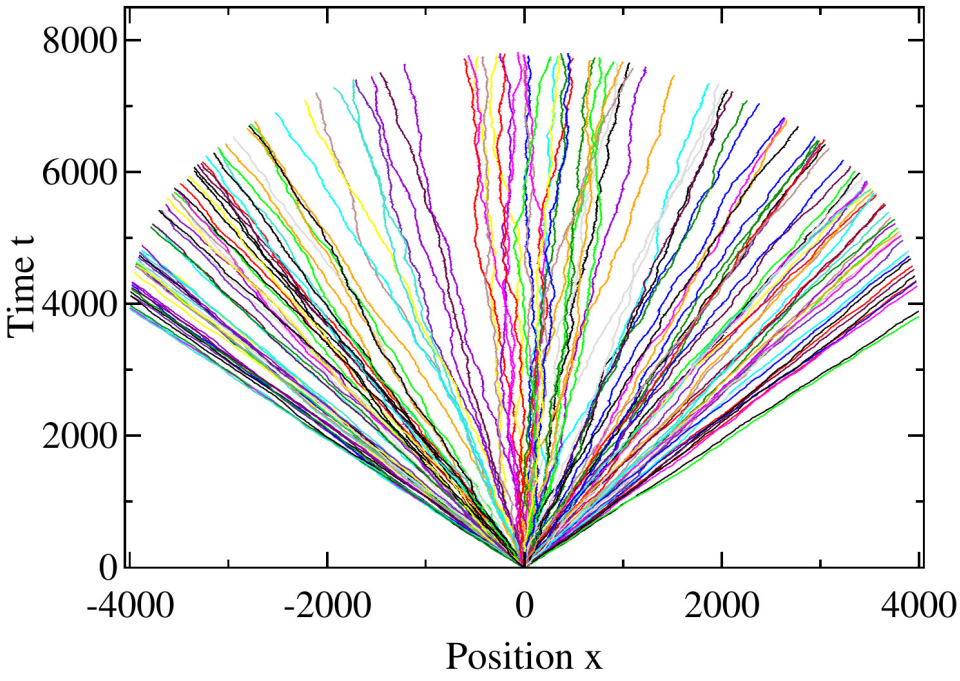

Figure 2.2: Trajectories of second class particle in the TASEP Speed Process. 150 different trajectories consisting of 4000 steps taken by the second class particle have been plotted.

and time, in the absence of the second-class particle.

2. Then we try to describe the motion of the second class particle moving as a random walk in a space-time-dependent background field $\rho(x,t)$.

We show that this simple description captures essential features of TSP and allows for further analysis.

Let $x(t)$ denote the position of the second class particle at time t. We want to discuss the stochastic properties of this trajectory, by integrating out all the first-class particles. The hydrodynamics of TASEP was first studied by Rost [17]. The coarse-grained evolution of the sea of first class particles in terms of particle density $\rho = \rho(x,t)$ can be described by the partial differential equation:

$$\frac{\partial \rho}{\partial t} + (1-2\rho)\frac{\partial \rho}{\partial x} = 0 \tag{2.1}$$

with

$$\rho(x, t=0) = \theta(-x),$$

where $\theta(x)$ is the step function, which is 0 for $x < 0$, and 1, for $x > 0$. The solution of this

partial differential equation is obtained to be:

$$\rho(x,t) = 1 \qquad for \qquad x < -t \tag{2.2}$$

$$\rho(x,t) = 0 \qquad for \qquad x > t \tag{2.3}$$

$$\rho(x,t) = \frac{1}{2}(1 - \frac{x}{t}) \qquad for \qquad -t \leq x \leq t \tag{2.4}$$

The motion of the second class particle is described by a stochastic differential equation

$$\frac{dx}{dt} = \bar{V}(\rho(x,t)) + \eta(t) \tag{2.5}$$

where $\bar{V}$ equals the mean velocity of the particle, and $\eta(t)$ takes into account all the fluctuations away from the mean. By definition, $< \eta(t) >= 0$. $\bar{V}$ is an externally prescribed function of ρ in Eq(5). In our problem, $\bar{V} = 1 - 2\rho$, where rho is given by Eq(4). Hence we write

$$\bar{V}(\rho(x,t)) = 1 - 2\rho(x,t) \tag{2.6}$$

Substituting the value of $\rho(x,t)$ from above:

$$\frac{dx}{dt} = \frac{x}{t} + \eta(t) \tag{2.7}$$

This is a linear differential equation, and may be solved by using an integrating factor. Equivalently, we make a change of variables to $v(t) = x(t)/t$, the mean velocity of the particle. This satisfies the simpler equation

$$\frac{dv(t)}{dt} = \frac{\eta(t)}{t} \tag{2.8}$$

This is easily solved to give

$$v(zT) - v(T) = \int_{T}^{zT} \frac{\eta(t')}{t'} dt' \tag{2.9}$$

As η, by definition has zero mean and z is a real number greater than 1. This gives $< v(zT) >=< v(T) >$.

We can also determine the variance of $v(T)$:

$$\left\langle (v(zT) - v(T))^2 \right\rangle = \int_{T}^{zT} \int_{T}^{zT} \frac{< \eta(t')\eta(t'') >}{t't''} dt'dt'' \tag{2.10}$$

We expect correlation function $< \eta(t)\eta(t') >$ to be short-ranged. It was shown for TASEP in [18] that correlations $< \rho(x,t)\rho(x',t') >$ are exponentially decreasing in time $|t-t'|$, unless x and x' are such that $x - x' = u(t-t')$, where u is the mean velocity of the flow. In our case, we easily see that while the second-class particle sees a constant density, the mean velocity of first class particles is $1-\rho$, and of second class particle is $1-2\rho$, and they are not equal. So, in general, the correlation function is short-ranged, and if $D = \int_{-\infty}^{+\infty} d\tau < \eta(t)\eta(t+\tau) >$, we may write $< \eta(t)\eta(t') >= D\delta(t-t'))$, which gives

$$< [v(zT) - v(T)]^2 >= \frac{D(z-1)}{zT} \tag{2.11}$$

which goes to 0 as T increases. This shows that the velocity of the second-class particle does get fixed at large T.

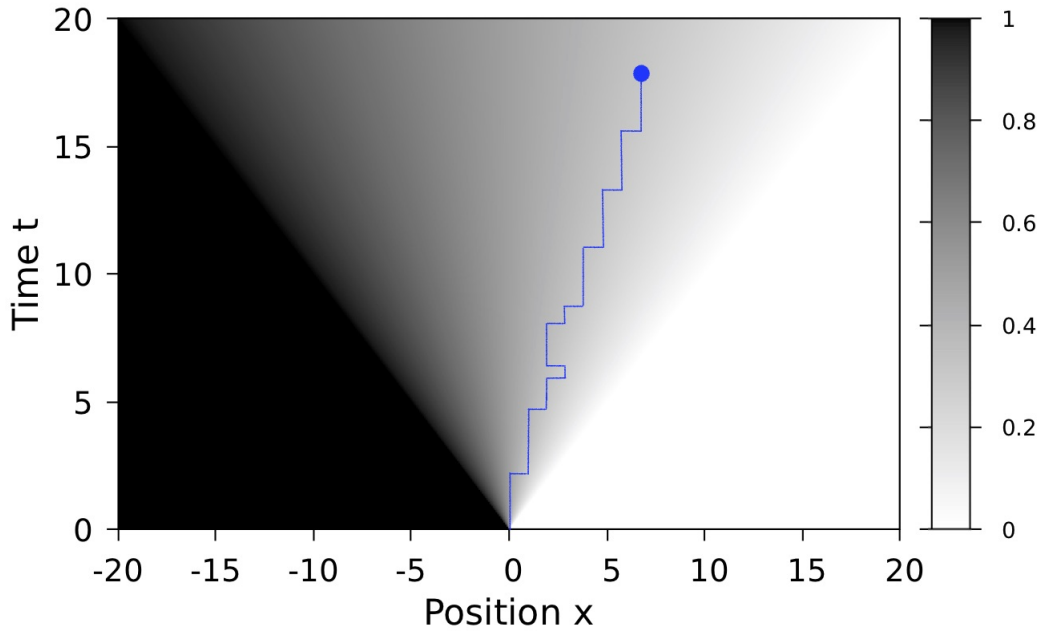

Figure 2.3: A schematic representing the motion of the second class particle (blue) in the space-time dependent background density plotted as a heat map.

2.4 Approximate random walk descriptions of the trajectory

While the Langevin description correctly describes the long-time behavior of trajectory correctly, the actual walk occurs on a discrete lattice, and a more accurate description would be as a random walk on a line in continuous time. This we will try to develop now.

2.4.1 Simple Biased Random Walk

In the spirit of the discussion above, consider motion of a second class particle in uniform density ρ. The trajectory then has mean velocity $U = 1-2\rho$, and its time evolution for times $t >> 1$ can be discussed as a simple random walk. It is known that if there is no second class particle, then in the steady state, occupation numbers of TASEP have a product measure. Then, in the steady state of TASEP, with a fixed density ρ, if we assume that we place a second class particle, with prob. $(1-\rho)$, its site on the right will be empty, and then it jumps with rate 1. Similarly, with probability ρ, the site on its left will be occupied and it will overtake the second class particle with rate 1. So, we conclude that trajectory of particle is a biased random walk. On a background density $\rho(x,t)$, the second class particle jumps to the left with rate $\rho(x,t)$, and to the right with rate $1-\rho(x,t)$. As a check, the mean velocity is $U = 1-2\rho(x,t)$, which agrees with the exact asymptotic value of velocity [19]. We have simulated this walk on the background $\rho(x,t)$ given by Eq(2.2-2.4). The results are shown in Figure 2.4. We also compare with the the simulation of the original process (Figure 2.2). We see that while we do get trajectories with velocity fixation, and the velocity U is uniformly distributed in the interval $[-1,1]$, the time taken by the walker to take 4000 steps is roughly the same while, the time taken in TSP shows a clear ρ dependence.

2.4.2 Markovian Continuous Time Random Walk

This shows that the rates of left and right jumps in our simple approximate model do not correctly describe the trajectories of the original problem. The difference occurs because the average density of first class particles near the second-class particle is not the same as in the bulk, away from the second class particle. Hence our approximation of using the steady state

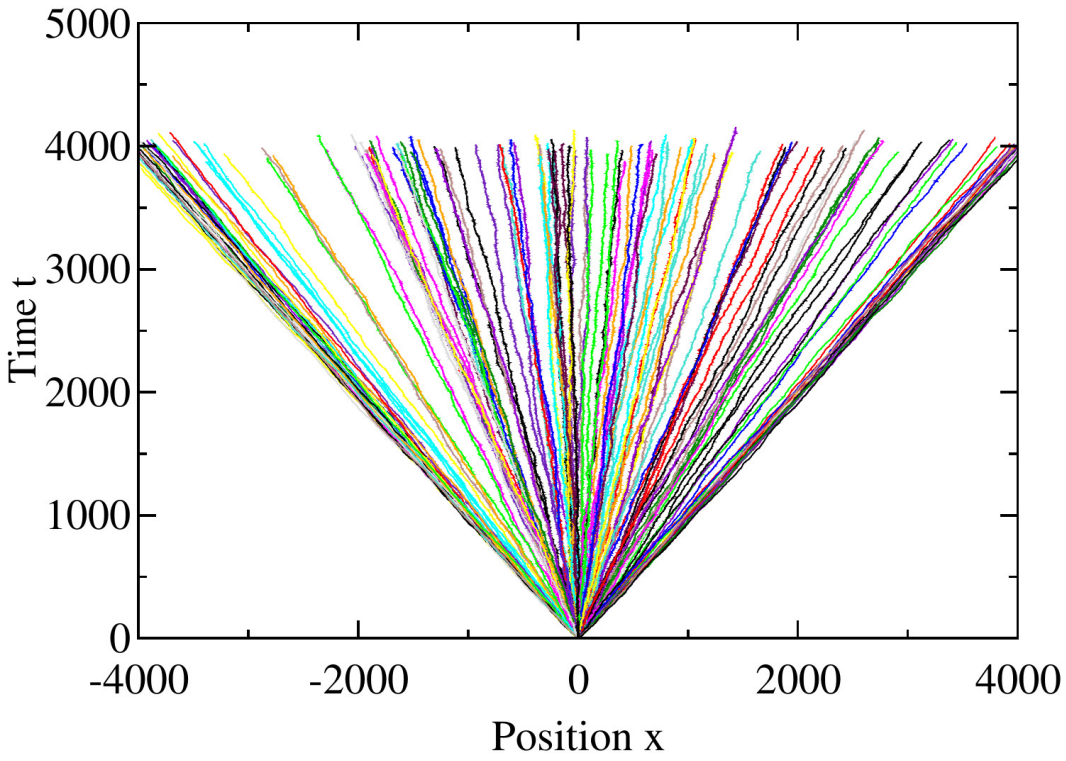

Figure 2.4: Trajectories of a CTRW with rate $\rho(x,t)$ of jumping to the left and $1-\rho(x,t)$ of jumping to the right. 150 different trajectories consisting of 4000 jumps made by the random walker have been plotted. Notice that the time taken by the walker to take 4000 jumps is roughly the same in each trajectory which is not the case in TSP.

measure of TASEP to calculate jump rates in the problem with a second class particle is present not adequate. The average density profile near a second class particle in the steady state has been calculated in [20] using the matrix product ansatz. It was shown that the second class particle is attracted to regions with a positive density gradient. More precisely, it was found that for a second class particle on a ring with density ρ of first class particle, in the steady state, the mean density on the site to the right is $2\rho - \rho^2$ and on the site to the left is ρ^2. This implies the probability of the site to the right being empty is $(1-\rho)^2$. If we use a continuous time random walk model with jump rates $(1-\rho)^2$ to the right and ρ^2 to the left we still get mean velocity $= 1-2\rho$. But now the agreement with the simulations is much better as seen in Figure 2.5.

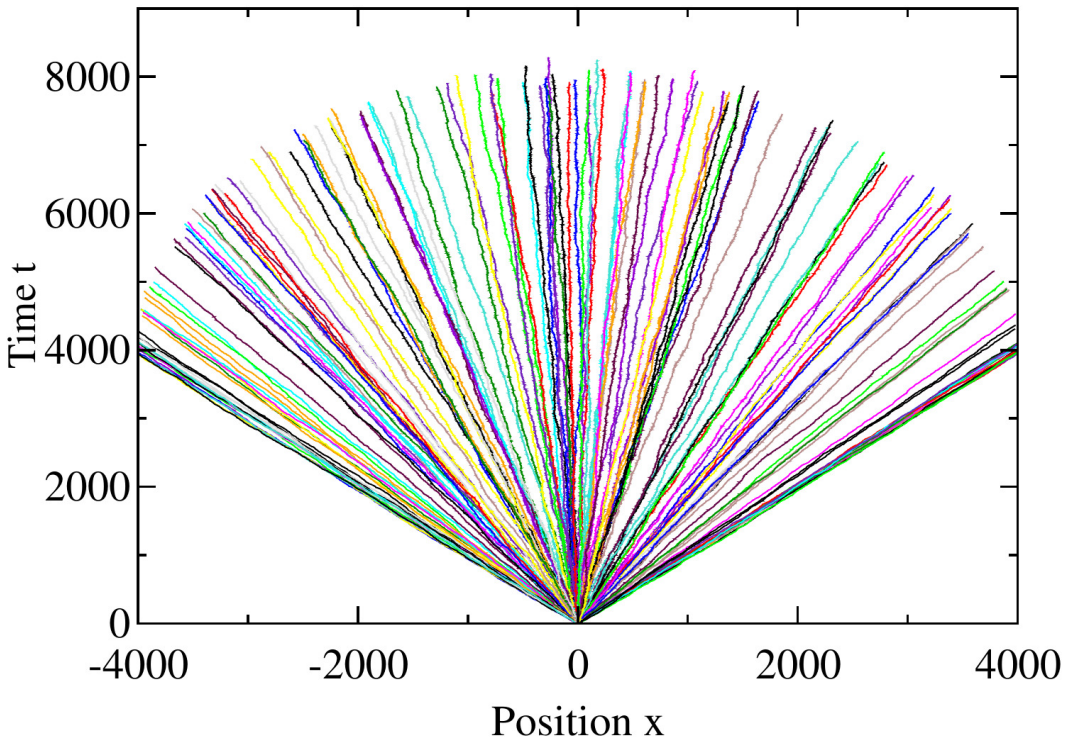

Figure 2.5: Trajectories of second class particle in the CTRW model with jump rates $(1-\rho(x,t))^2$ to the right and $(\rho(x,t))^2$ to the left. 150 different trajectories consisting of 4000 steps taken by the second class particle have been plotted.

2.4.3 Continuous Time Random Walk with Waiting Time Distributions

However, our description is still not sufficiently accurate. If we are given a single long trajectory of the second-class particle, with mean velocity U in the original process between times T and nT, for $T >> 1$, and also one generated using the Markovian jump rates descibed above, can one distinguish between them? The answer is *yes*. Clearly, in the Markovian approximation, the waiting times between successive jumps are independent random variables, with a distribution that is a simple exponential. One can easily verify that in the original process the waiting time intervals do not have an exponential distribution. This comes from the fact that since occupancy of neighbors by first class particles have non-trivial correlations in time, so the probabilities of jump in nearby time intervals $[t, t+\Delta t_1]$ and $[t+\Delta t_1, t+\Delta t_1+\Delta t_2]$ are not uncorrelated.

The trajectories in the TASEP Speed Process show a nearly exponential distribution

of waiting times only for velocities close to 1 and -1 whereas a clear departure from the exponential distribution is observed for smaller velocities. Figure 2.6 shows the distribution of waiting times for the TSP and the CTRW model. The histograms were plotted for two trajectories, consisting of 8000 steps taken by the second class particle, of velocity (a) 1 and (b) 0.2. It is clearly seen that an even more accurate modelling of the trajectory will be as a random walk which involve a continuous time non-Markovian walk with a prescribed distribution of residence times $f(\tau)$, with probability to jump left or right given by $p(\tau)$ and $1-p(\tau)$. The calculation of the exact functions $f(\tau)$ and $p(\tau)$ is rather difficult, and will not be attempted here. We can take these to be approximately determined from simulations.

Of course, even this modelling of the trajectory as a continuous time random with a distribution of waiting times is approximate. In the original process, the waiting times between successive jumps are only approximately uncorrelated. But going beyond this description falls outside our aim of providing a simple approximate description of the trajectories.

2.5 Extensions of our approach

This work can be extended to the case of a multi-species *partially* asymmetric exclusion process (ASEP). It was conjectured in [2] that even in partially asymmetric case, the asymptotic velocity tends to a uniformly distributed random variable. More precisely, in this case, if we start with the initial conditions as before and look at the motion of the second class particle, then:

$$\frac{X(t)}{t} \xrightarrow{t \to \infty} U_p$$

where $X(t)$ is the position of the second class particle at time t and U_p is a uniform random variable between $[-(2p-1),(2p-1)]$ where p is the rate of jumping to the right ($1-p$ being the rate of jumping to the left). An Langevin description can be developed for this as the evolution of density for first class particles is given by:

$$\frac{\partial \rho(x,t)}{\partial t} + (2p-1)(1-2\rho(x,t))\frac{\partial \rho(x,t)}{\partial x} = 0$$

Even in the case of multi-species ASEP, our analysis goes through and the fluctuations about the average velocity die out as t^{-1}.

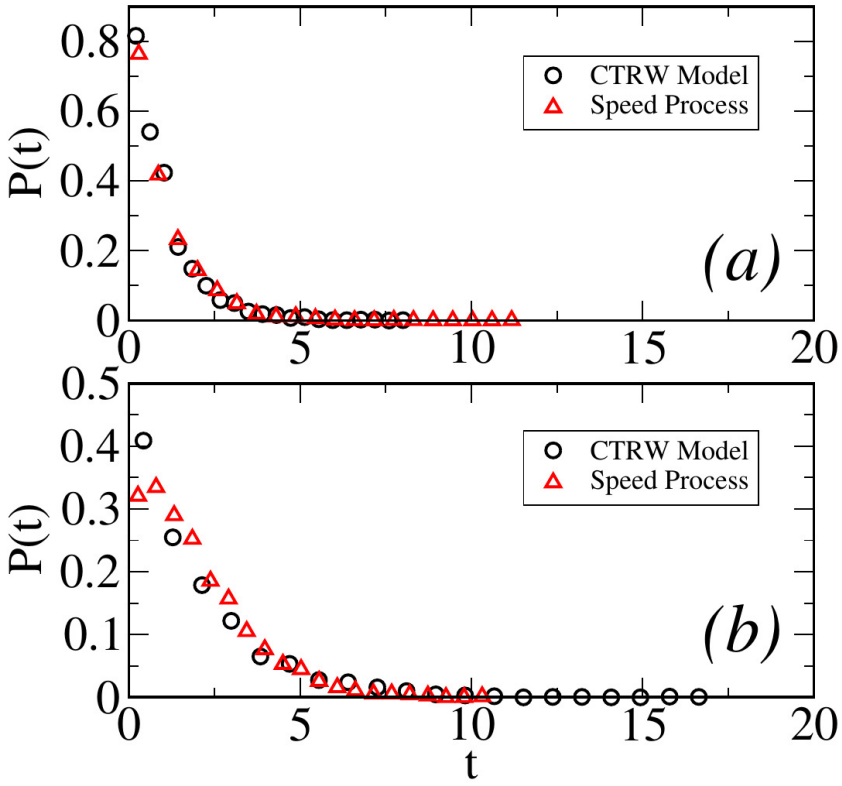

Figure 2.6: Waiting time distributions for trajectories with speeds (a) 1 and (b) 0.2 in the CTRW model (black circle) and the TASEP Speed Process (red circle). For speeds close to 1, the waiting time distribution for the TASEP Speed Process matches closely with the exponential waiting times of the CTRW model. However, for intermediate speeds, a clear departure from exponential waiting time distribution is observed.

The finite lattice version of the multi-species problem [21] offers an interesting extension to the effective medium approach. The system considered is a finite lattice with n sites in which, each site is occupied by a particle and its class is labeled by its initial position on the lattice. The time evolution of the system is given by the stochastic nearest neighbor exchange rule:

$$ij \xrightarrow{rate\ 1} ji \quad \text{for all } i < j$$

If we wish to study the dynamics of a tagged particle of the k-th class, it is clear that the problem is, again, reducible to a two species problem with particles of l-th class ($l < k$) being equivalent to first class particles, particles of m-th class ($m > k$) being holes and the tagged particle being the second class particle.

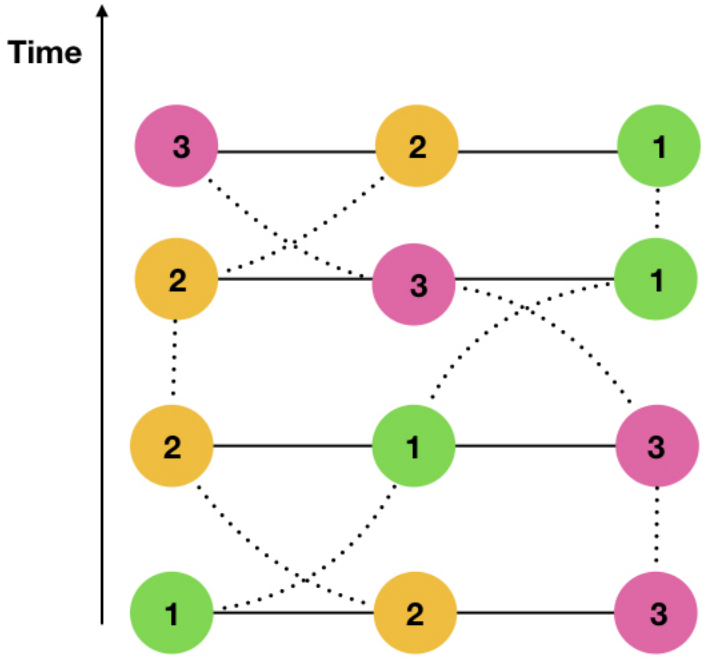

Figure 2.7: A realization of the finite lattice process with 3 particles.

The motion of a tagged particle is strongly affected by the ends and displays an interesting behaviour - initially, its dynamics of the tagged particle mimics the dynamics of a tagged particle in TSP on an infinite line. However, at later times, the particle reaches a growing impenetrable region of density 1 (0) on the right (left) and travels along with it, remaining at the moving end of this region at subsequent times, till its absorbing position. This is expected as the lattice is finite and after some time, clearly the first class particles (holes) start to get accumulated at the right (left) boundary. Figure 2.8 is a schematic of this evolution. It is interesting to note that the absorbing position of a particle whose initial position was k is always $n-k$. This behaviour can be described by CTRW model with jump rates given by the following background density:

$$\rho(x,t) = \begin{array}{lll} 0 & for & x \leq l(t) \\ 1 & for & x \geq n - r(t) \\ \frac{1}{2}(1 - \frac{x-k}{t}) & for & -t + l(t) < x - k < t - r(t) \\ 1 & for & l(t) \leq x < k - t + l(t) \\ 0 & for & k + t - r(t) \leq x < n - r(t) \end{array} \tag{2.12}$$

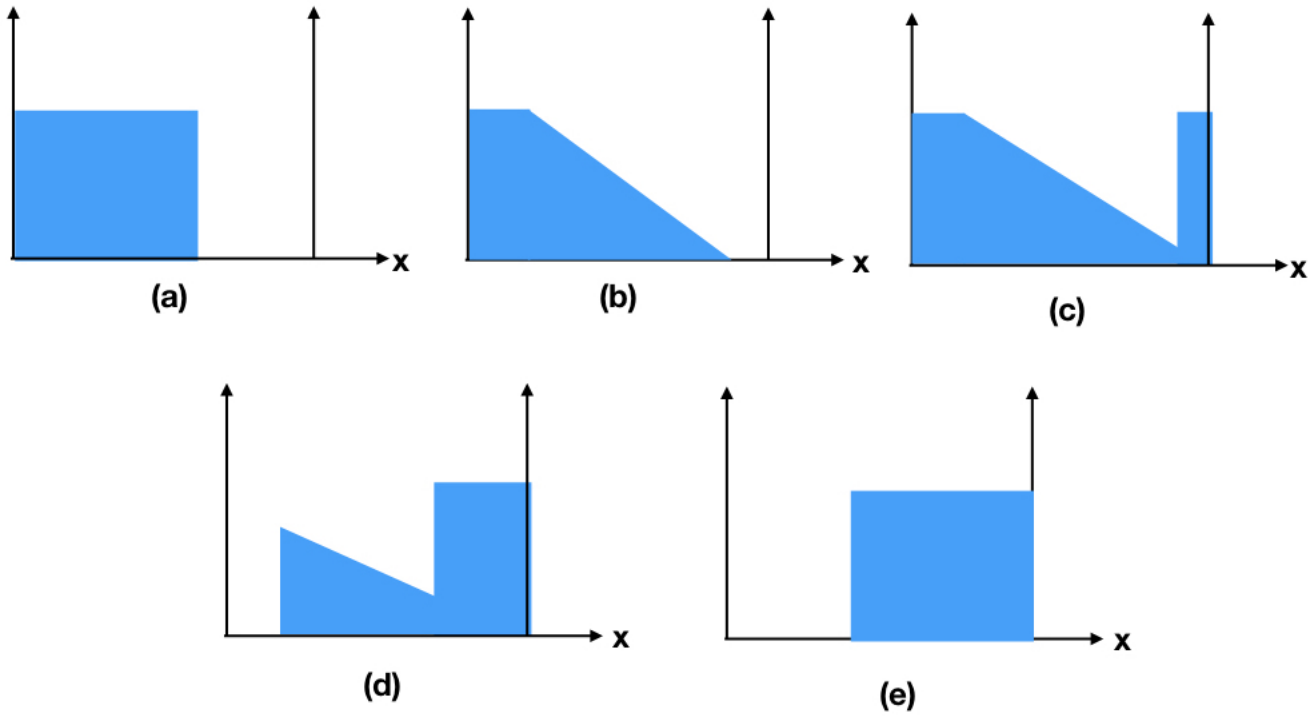

Figure 2.8: Density profiles at various times: (a)$t = 0$, the process hasn't started; (b) positive t, no finite size effects felt so far; (c) and (d) regions of density 1 and 0 start to form on the right and the left sides respectively; (e) the process ends.

The fact that the density of first class particles evolve in such a way was elegantly obtained in [5]. $l(t)$ and $r(t)$ are the mean widths of impenetrable regions of density 1 and 0 on the right and left boundary respectively and they satisfy:

$$\begin{aligned} r(t) = & \quad 0 & for & \quad t \leq (n-k) \\ & t + (n-k) - 2\sqrt{t(n-k)} & for & \quad t_s \geq t > (n-k) \\ & \quad k & for & \quad t > t_s \\ l(t) = & \quad 0 & for & \quad t \leq k \\ & t + k - 2\sqrt{tk} & for & \quad t_s \geq t > k \\ & \quad n-k & for & \quad t > t_s \end{aligned} \tag{2.13}$$

where t_s is the mean time taken by the tagged particle to reach its absorbing position and is given by $t_s = n + 2\sqrt{k(n-k)}$.

We simulated the process on a lattice of 1000 sites and looked at the various trajectories of the particle labelled 200. Figure 2.9 shows 150 such trajectories and Figure 2.10 shows analogous results for the effective medium description using a continuous time random walker on a line with jump rates determined by the background density given in Eq(2.12).

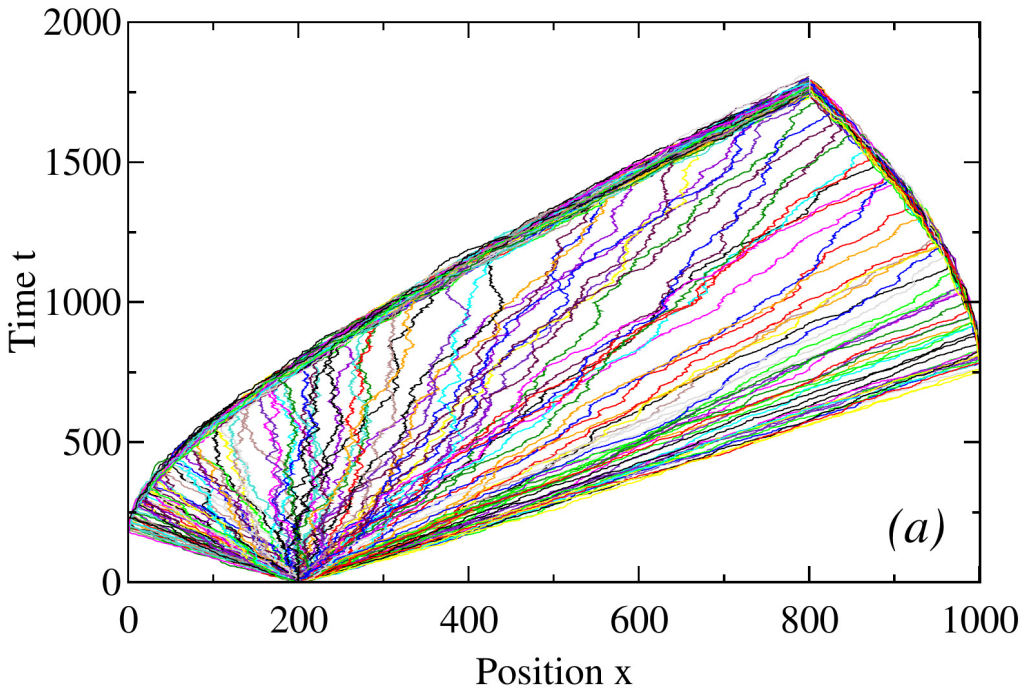

Figure 2.9: 150 different trajectories of the particle labelled 200 in the finite lattice version of TSP with 1000 particles.

As an interesting variation to the multi-species problem, consider a 1D lattice where each lattice site is occupied with a particle and the class of each particle is labeled by its position on the lattice with only the following nearest neighbor transitions allowed:

$$ij \xrightarrow{rate\ (j-i)^{\alpha}} ji \quad \text{for all } i<j$$

This model is clearly a better model for traffic flow if we visualize the x-coordinate of particles to not be their position in real space, but their relative order on the road as the overtakings between two particles happen at rates proportional to the difference between their labels (which is a proxy for the velocity).

Some special cases of this model have been studied before [6 – 8]. It is known that the steady state of such a model on a 1D lattice with open boundary conditions and $\alpha = 1$,

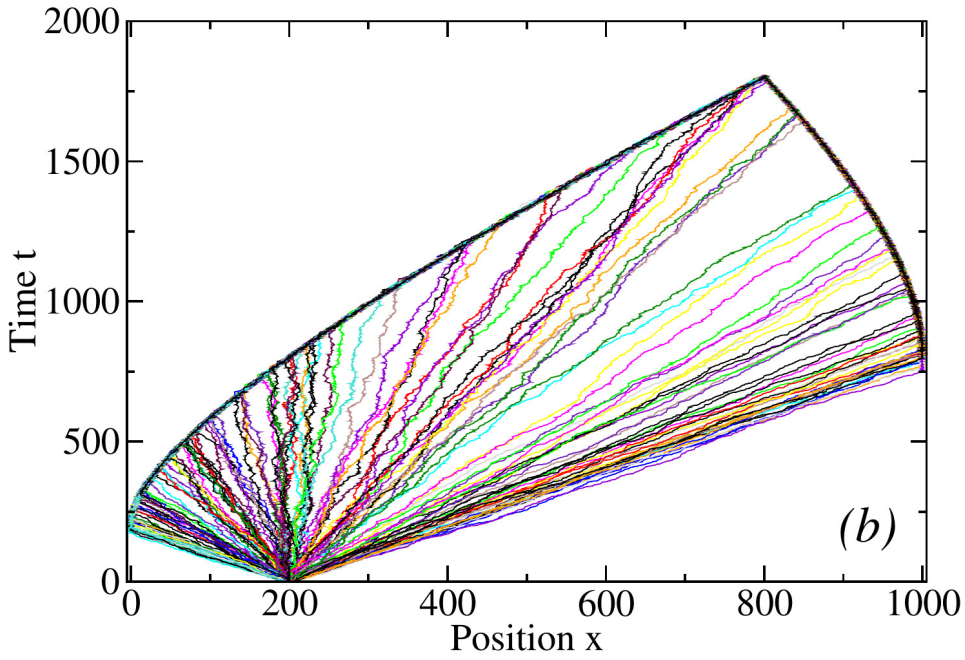

Figure 2.10: Trajectories of a continuous time random walker with space time dependent jump rates determined by the evolving density of first class particles defined by Eq(2.12)

in which there was an additional feature that particles could enter the system from the left end and leave from the right at rates depending on their labels, can be obtained by a matrix product ansatz. This was later generalized to obtain the steady state properties of this system on a ring. We consider the dynamics of a tagged particle in this modified multi-species exclusion process on an infinite line for a general α where particles do not enter or exit the system. This problem cannot be reduced simply to the 2-species problems as each particle interacts with every other particles differently. However, we find that something analogous to the "velocity selection" in TSP happens in this process as well. The trajectories of the tagged particle in this process seem to belong to the family of curves $t = ax^{1-\alpha}$ for $\alpha \neq 1$ and $t = \ln ax$ for $\alpha = 1$ where a parametrizes the trajectories. A heuristic argument for this is as follows:if a particle has moved distance x in time t, then the typical change in velocity it encounters with its neighbor is proportional to x. Then $dx/dt \sim x^{\alpha}$ implies that $x \sim t^{1/(1-\alpha)}$. for $\alpha \neq 1$ and $t \sim \ln x$ for $\alpha = 1$.

We demonstrate numerical results in Figures 2.11 and 2.12 for $\alpha = \frac{1}{2}$. Figure 8 shows 150 different space-time trajectories of the process and Figure 9 shows the trajectories when the time coordinate t is scaled as $\frac{t}{2\sqrt{x}}$ where we have only chosen the trajectories whose displacement always remains positive. We see that $t/\sqrt{x}$ is nearly constant for each trajectory,

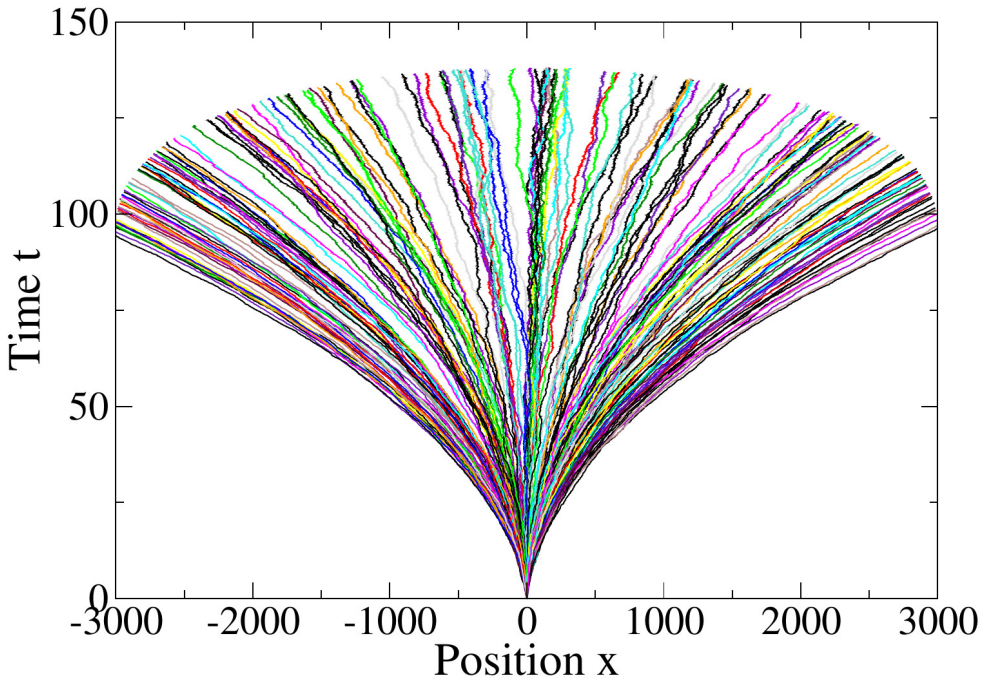

Figure 2.11: 150 trajectories consisting of 3000 jumps made by a tagged particle in the modified multi-species exclusion process with $\alpha = 0.5$.

but different trajectories have very different values of this variable. Finding the distribution of the asymptotic value of a over different trajectories remains an open problem.

2.6 Summary

In summary, we discussed the effective medium approach to describe the motion of a tagged particle in the time-evolving background other particles. We provided a simple Langevin description of the dynamics, that captures the key features of the large-scale behavior of TSP, and also calculated the variance of the average velocity within one history, and for different histories. We discussed how to improve the effective medium description to take into account different additional features of the trajectories. These were approximating the trajectory as a biased random walk, with rates of walk calculated from the steady state of the TASEP, in the absence of the second-class particle. We found that to get a quantitative agreement with the original process, one has to incorporate the modification of the average density profile that occurs near the second-class particle. Also, while the time evolution of

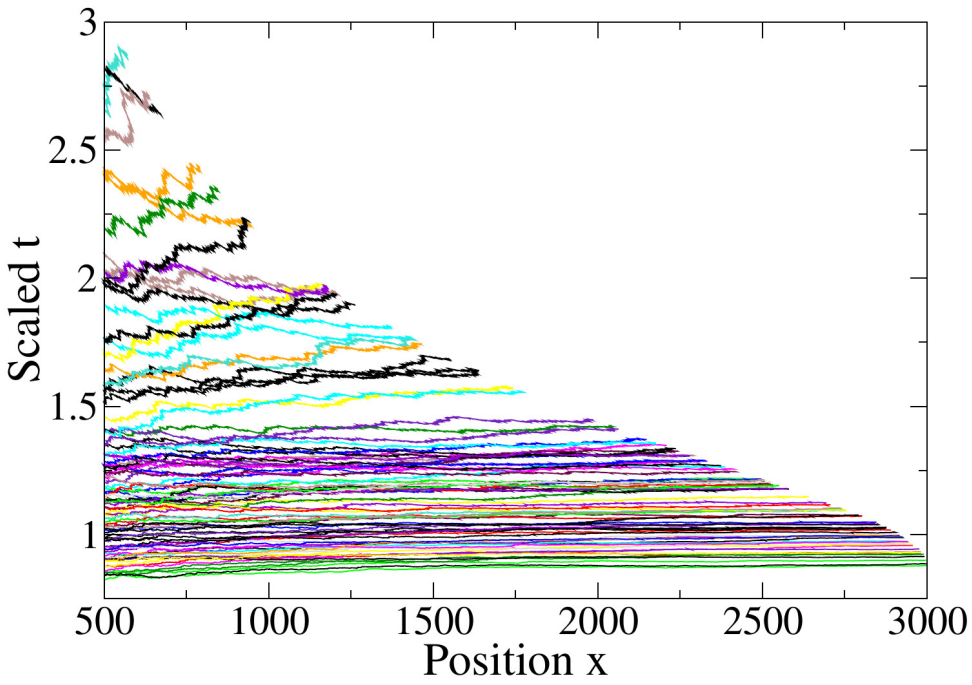

Figure 2.12: Trajectories of the tagged particle in the modified multi-species exclusion process with $\alpha = 0.5$ after time coordinate t is scaled as $\frac{t}{2\sqrt{x}}$. 150 different trajectories are plotted showing that all the trajectories belong to a family of curves given by $t \sim \sqrt{x}$.

the original process was Markovian by definition, the evolution of the projected process is non-Markovian. This is most easily seen in the non-exponential distribution of waiting times between jumps in the motion of the second-class particle. We proposed a non-Markovian continuous time random walk with a distribution of waiting times between jumps as a good description of this. We later extended our approach to a finite lattice version of the TSP and studied the trajectories of a tagged particle in this process. In this case, interesting end-effects are seen which can also be explained within the effective medium approach. Lastly, we looked at a modified multi-species exclusion process in which exchanges between adjacent particles happened at rates proportional to the difference in their labels. We showed that in this process too, the motion of a tagged particle shows a behaviour in which it initially chooses a trajectory from a family of curves and sticks to it asymptotically. A better understanding of our heuristic arguments, and numerical observations about this process for a general α seems to be an interesting problem for further study.

Chapter 3

The Asymptotic Shape of Eden Clusters

From bacterial colonies and growing tumors to forest fires and spreading of rumors, phenomena of cluster growth can be seen everywhere. While studying models of these processes, it is natural to ask about the spatial extent of the growing cluster at any given time t. Given that there is a disease outbreak, in what regions should you focus your immunization programs? Or given that a rumor has been started by a specific person, who are the people to whom the rumors would have reached? In this chapter, we will provide a method to answer such questions, in the context of the *Eden model.*

3.1 Introduction

In Chapter 3, our main focus would be studying the stochastic evolution of a growing surface or cluster. There has been a lot of interest in the study of stochastic growth models in recent years [5, 15, 23, 25, 29] – mainly owing to their ubiquity and partly to their beauty. With the recent advances in network theory and stochastic processes, there is a growing interest in studying spreading phenomena in complex heterogeneous environments. However, there still is a lot left to understand in the simplest model, defined on a regular lattice, called the Eden model [32]. Important questions that are yet to be addressed are based on studying the long time asymptotics of its dynamics. One such question is understanding the asymptotic shape

of the growing cluster. In this regard, in the context of the Eden model, bounds on velocity of the growing cluster along the axis and the diagonal directions have been obtained earlier [24, 25, 28]. In the context of this epidemic process, the question of finding upper bounds to the shape of the growing cluster is natural, and is equivalent to estimating the size of region in which the residing people could be exposed to a particular infection given that the patient zero resides at the origin. As far as the shape is concerned, most studies have been concerning the inequality of velocity along the axes and diagonal [26, 30]. While some numerical studies of the asymptotic shape have been reported in 2 dimensions, we could not find any discussion of the equation of the asymptotic shape. Here, we find the upper bounds on the growth velocity in a general direction on d-dimensional hypercubical lattice.

3.2 The Eden Model

We begin by defining the Eden model as an epidemic model. Consider an infection process on a $d-$dimensional hypercubical lattice where each site can either be infected or healthy. We denote the coordinates of each site by $(x_1, x_2, ..., x_d)$. At time $t = 0$, only the origin O=$(0, 0, ..., 0)$ is infected and all other sites are healthy. The evolution is a continuous time Markov process in which an infected site infects its healthy neighbours at rate 1. We consider the process in which an infected site never recovers. This model is equivalent to first passage percolation with exponentially distributed independent passage times.

This model was first introduced by Murray Eden in 1961 [32] to investigate the growth of biological cell colonies. Many variants of this model have been studied since then − starting from the model of skin cancer by Williams and Bjerknes [31] to the SIR (Susceptible-Infected-Recovered) and SIS (Susceptible-Infected-Susceptible) models of epidemics. Apart from the many applications that one can think of, surface growth models, in general, have given us a lot of insight into nonequilibrium phenomena by providing us with a platform to study universal behavior [29].

With this motivation in mind, we start our discussion on the shape of Eden clusters.

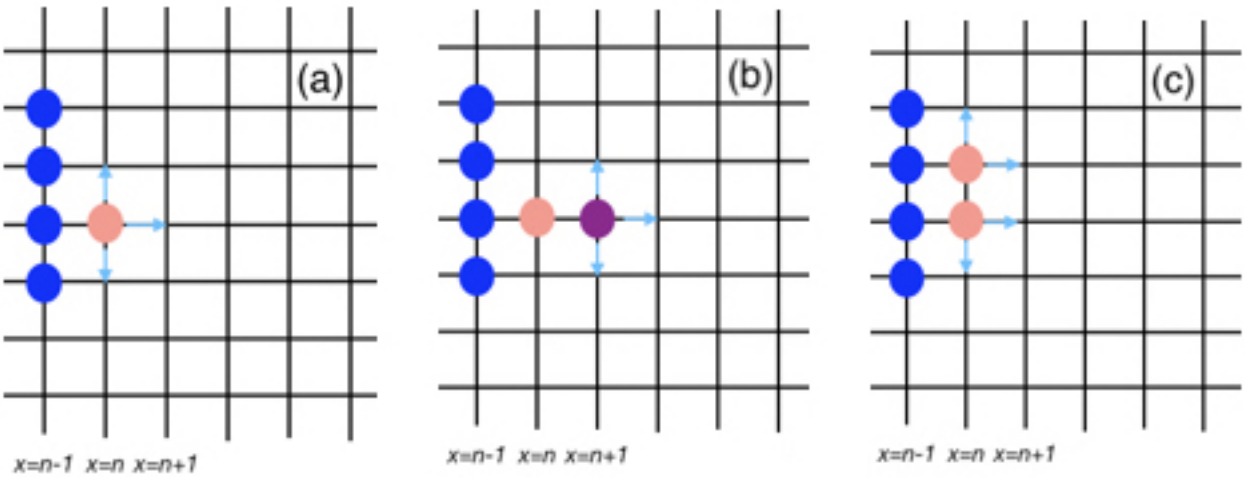

Figure 3.1: The idea behind finding a lower bound to the velocity of the Eden front.

3.2.1 Lower bound to velocity of the Eden front along axis in 2D

Before addressing the question of upper bounds to the velocity of Eden front in any general direction, we will provide an analytical method to obtain a lower bound on the velocity along the axis in two dimensions.

The idea is as follows: Consider the semi-directed Eden process in which infections can traverse along the positive and negative $y-$ axis and the positive $x-$axis we want to find the time taken to infect any lattice point on the line $x = n + 1$ given that the first infection on the line $x = n$ just happened. Suppose, all the infected sites on the lines $x = k$ for $k < n$ become dead as soon as a site on $x = n$ is infected (dead sites can't infect their neighbors any further). It is clear that, in this modified process, the time taken to infect any lattice point on the line $x = n+1$ after the first infection on the line $x = n$ happened will be greater than the time taken in the Eden model for the same. This idea was presented originally by Kesten to refute the Eden conjecture but he could only show it for dimensions larger than 10^6. Recently, Bertrand and Pertinand [24] used this idea and improved bounds on the velocity along axis and significantly decreased the upper bound on the number of dimensions in which the Eden conjecture does not hold to 22. Figure 3.1 demonstrates the idea behind finding this bound in $2D$. In 3.1(a), the line $x = n$ has just been infected (orange). The deep blue particles on the line $x = n - 1$ are now dead and cannot infect any further. The dynamics is now constrained only to the lines $x = n$ and $x = n + 1$. Let T_1 denote the time taken to first infect line $x = n + 1$ starting from the configuration shown in 3.1(a). Clearly,

there are only two possibilities for the next step: either the infection spreads further on the $x = n$ line (3.1(c)), or it infects the line $x = n + 1$ (3.1(b)). It is easily seen that T_1 satisfies the following equation

$$T_1 = \frac{1}{3}.\frac{1}{3} + \frac{2}{3}.\left(\frac{1}{3} + T_2\right)$$

Where T_2 denotes the time taken to first infect line $x = n+1$ starting from the configuration shown in 3.1(c) where there are two adjacent infected sites on the line $x = n$. Similarly, we can define T_N as the time taken to infect the line $x = n + 1$ starting from the configuration where there are N adjacent infected sites on the line $x = n$. Then

$$T_2 = \frac{1}{4}.\frac{2}{4} + \frac{2}{4}.\left(\frac{1}{4} + T_3\right)$$

and we have the general recursion relation

$$T_N = \frac{1}{N+2}.\frac{N}{N+2} + \frac{2}{N+2}.\left(\frac{1}{N+2} + T_{N+1}\right)$$

This recursion relation can be solved to give $T_1 = 0.5973$, which is an upper bound on time taken for a line to infect its adjacent line. Equivalently, $1/T_1 = 1.674$ gives a lower bound on the velocity of the Eden front along the axis.

We will now shift our discussion to upper bounds to the asymptotic shape of the Eden cluster using the Independent Branching Process (IBP) and its variants. But first, we will define the IBP.

3.3 The independent branching process

The independent branching process (IBP) on the Z^d lattice is defined as follows: We consider an infection process in which the number of cells present at a site can be arbitrarily large. Let $n(\vec{R}, t)$ denote the number of cells present at the site $\vec{R}$ at time t. At the time $t = 0$, there is only one cell present in the system, and it is placed at the origin $\vec{O}$. Then, we have $n(\vec{R}, t = 0) = \delta_{\vec{R},\vec{O}}$.

The time evolution is a continuous-time Markov process. At any time t, a cell can give birth to a descendant cell, that sits at a nearest neighbor site. Then number of cells at the

neighbor increases by one. Once born, a cell never dies. We assume that the rate at which a cell gives birth to a daughter cell is 1 along each bond, independent of the number of cells present at the site, or at neighbours.

In this model, the number of cells present at time t increases exponentially with t. Each cell gives birth to a daughter cell at a rate $2d$ per unit time (because each has $2d$ neighbors). Hence the average number of cells present at time t is $\exp(2dt)$, for all $t > 0$. Also, with time, the region occupied by at least one cell, also called the region invaded by the cells, grows with time. The outer boundary of the region invaded by the cells is called the invasion front. We define $u(\vec{\Omega})$ as the velocity of the invasion front in the direction $\vec{\Omega}$ as

$$u(\vec{\Omega}) = \lim_{t\to\infty} (1/t)\ \vec{R}_t(\vec{\Omega}) \tag{3.1}$$

where $\vec{R}_t(\vec{\Omega})$ is position of the invasion front in the direction $\vec{\Omega}$) at time t. It is easily seen that $u(\vec{\Omega})$ has a non-zero limit, and the fluctuations in $(1/t)\ \vec{R}_t(\vec{\Omega})$ tend to zero as time increases.

In the Eden process(EP), the number of cells at any site is at most 1. It is easily that if we have two configurations $\mathcal{C}$ and $\mathcal{C}'$, where $\mathcal{C}$ evolves according to the rules of EP, and $\mathcal{C}'$ evolves as an IBP, and at any given time t, the number of cells in $\mathcal{C}'$ at any site $\vec{R}$ is greater than or equal to the number at the corresponding site in $\mathcal{C}$. Then, this property will be preserved at at subsequent times. This implies that the front velocity in IBP proves an upper bound to the front velocity in EP in all directions $\vec{\Omega}$.

It is straight forward to determine the growth velocity in IBP. Let the average number of cells in the IBP at time t, at the site $\vec{R}$ be denoted by $\bar{n}(\vec{R}, t)$. We use the fact that in IBP, these variables satisfy a linear equation

$$\frac{d}{dt}\bar{n}(\vec{R}, t) = \sum_{nn} \bar{n}(\vec{R}', t) \tag{3.2}$$

where the sum runs over the $2d$ nearest neighbors of $\vec{R}$. This is a linear equation, and is easily solved, by Fourier transformation. We define the variables $\tilde{n}(\vec{k}, t)$ as

$$\tilde{n}(\vec{k}, t) = \sum_{\vec{R}} \bar{n}(\vec{R}, t) exp(-i\vec{k}.\vec{R}) \tag{3.3}$$

Then, these variables satisfy the equation

$$\frac{d}{dt}\tilde{n}(\vec{k},t) = \lambda(\vec{k})\tilde{n}(\vec{k},t) \tag{3.4}$$

with $\lambda(\vec{k}) = 2\sum_{i=1}^{d} cos(k_i)$.

This equation is easily solved, and by inverse Fourier transformation, we get

$$\bar{n}(\vec{R},t) = \int \frac{d\vec{k}}{(2\pi)^d}\ \exp(\lambda(\vec{k})t + i\vec{k}.\vec{R}). \tag{3.5}$$

It is easily seen that for fixed $\vec{r}$, $\bar{n}(\vec{R},t)$ increases as $\exp(2dt)$. We are interested in the case where as t increases, $\vec{R}$ also becomes bigger with time as $\vec{R} = \vec{v}t$. Then, the integral becomes

$$\bar{n}(\vec{R},t) = \int \frac{d\vec{k}}{(2\pi)^d}\ \exp(t\left[\lambda(\vec{k}) + i\vec{k}.\vec{v}\right]). \tag{3.6}$$

In the limit of large t, this is evaluated easily, using the steepest descent method. The stationary point occurs at a imaginary value of $\vec{k} = i\vec{\kappa}$, given by

$$\kappa_j = \sinh^{-1}(v_j/2). \tag{3.7}$$

We define the large deviation function $F(\vec{v})$ by the condition that for large t,

$$\bar{n}(\vec{v}t,t) \sim \exp\left[tF(\vec{v})\right] \tag{3.8}$$

with

$$F(\vec{v}) = \sum_{i=1}^{d}\left[2\sqrt{1+{v_i}^2/4} - v_i \sinh^{-1}(v_i/2)\right] \tag{3.9}$$

We note that F is a decreasing function of its argument. At $\vec{V} = 0$, it has a value $2d$. And for large $|v|$, it varies as $-\sum_i |v_i| \log|v_i|$).

At the cluster boundary, $\bar{n}$ is of $\mathcal{O}(1)$. So, the boundary of the cluster, scaled by t, is given by equating the growth rate of $\bar{n}$ to zero. Thus, we get that the scaled boundary of

the cluster in the IBP is given by

$$\sum_{i=1}^{d} \left[2\sqrt{1 + {v_i}^2/4} - v_i \sinh^{-1}(v_i/2) \right] = 0. \tag{3.10}$$

Note that from Eq.(3.6), $\bar{n}(\vec{R}, t)$ is also equal to the number of walkers expected at $\vec{R}$ at time t, if $\exp(2dt)$ walkers are released at the origin at time $t = 0$, and perform independent random walks.

As a check, we see that along the diagonal direction $(1, 1, 1, 1..)$, we set $v_i = V_{diag}$, for all i. Then, for all d, we get V^* is the solution of the equation

$$2\sqrt{1 + {V_{diag}}^2/4} = V_{diag} \sinh^{-1}(V_{diag}/2) \tag{3.11}$$

which gives $V_{diag} \approx 3.01776$. This gives the well-known upper bound to the speed along the diagonal in d dimensions (measured in Euclidean norm) as

$$v_{diag,EP} \leq v_{diag,IBP} = 3.01776\sqrt{d}. \tag{3.12}$$

One can also verify that this agrees with the already known results about the asymptotic velocity along one of the axes in the IBP. In this case, we set $\vec{v} = (V_{axis,IBP}, 0, 0, 0..)$. The corresponding equation becomes

$$2\sqrt{1 + {V_{axis,IBP}}^2/4} + 2d - 2 = V_{axis,IBP} \sinh^{-1}(V_{axis,IBP}/2) \tag{3.13}$$

This is easily solved, and gives $V_{axis,IBP} = 4.4668, 5.67295, 6.75371$ and 7.75405, for $d = 2, 3, 4$ and 5 respectively. For large d, V_{axis} varies as $2d/log(d)$. These results about velocity along the axes, or along the main diagonal have been known some time. However, we could not find a discussion of the equation of the asymptotic surface. Numerically, Alm and Deijfen [26] studied the shape of Eden clusters. The new result here is the exact equation for the asymptotic shape of the cluster for the IBP, which provides an upper bound for the asymptotic cluster for the Eden process. In Fig. 3.2, we show the asymptotic shape in 3-dimensions calculated numerically using Eq.(3.10) In the EP, Alm and Deijfen found that the cluster shape is not exactly circular, with the Euclidean speed along the diagonal and

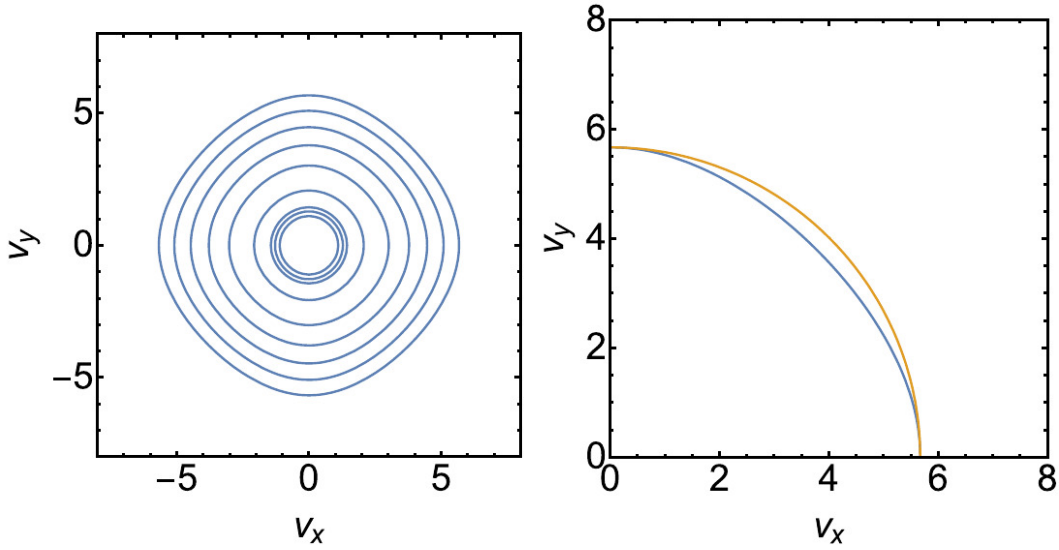

Figure 3.2: (a) A contour plot for the independent branching process in 3-D for $z = 0, 1, 2, 3, 4, 5, 5.5, 5.65$ starting with the outermost curve. (b) A demonstration of the departure from the spherical ball. The plot in blue is a numerical plot of equation (10) and orange is an arc of a circle with the radius 5.67

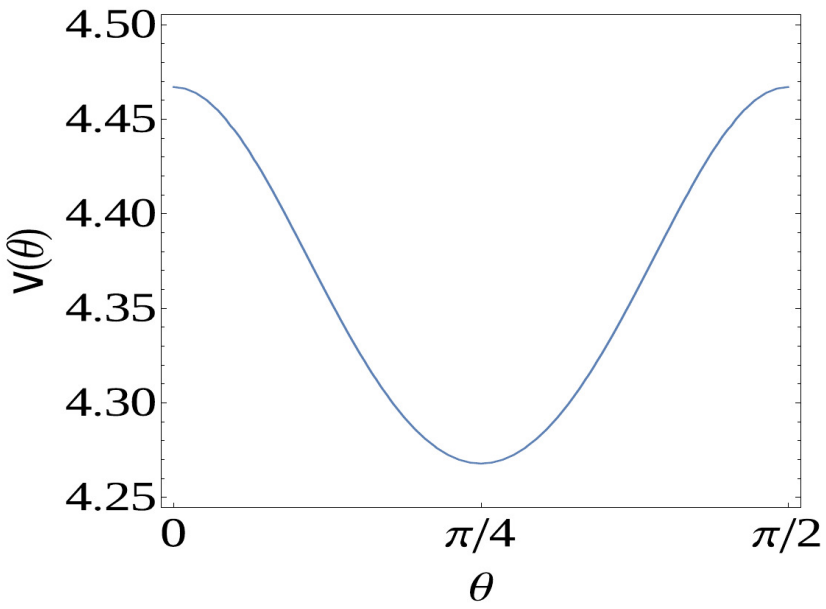

Figure 3.3: A plot of velocity v as a function of direction θ. Note that the velocity is maximum along the axis ($\theta = n\pi/2$ for integer n) and minimum along the diagonal direction ($\theta = (2n+1)\pi/4$).

along the axis being 2.4420 and 2.4742 respectively. Thus the speed along the diagonal is smaller by about 1.3%. For the IBP, we found these to be 4.26775 and 4.4668, with the diagonal speed being smaller that that along the axis by a bigger amount(about 4.5%).

3.4 Cluster shape in modified IBP$_1$

We will now define a model that is a bit more complicated than the IBP defined above. This is also a continuous-time Markovian evolution independent branching process. Here, we consider the process on a hyper-cubical lattice in d dimensions. The number of cells at any site can be a non-negative integer. As before, We start with a single cell at the origin at $t = 0$, with the rest of the lattice empty. However, We note that all cells, other than the original 'eve'-cell have a mother cell. The evolution rule is still Markovian. Each cell gives rise to a daughter cell along each bond at rate 1, independent of the state of the other sites, *except along the bond that connects it to its mother cell.* Thus, such a cell will have $(2d-1)$ bonds along which it can The 'eve'-cell gives rise to a child along all the $2d$ bonds connected to it, at rate 1. We call this process the Modified IBP1 (MIBP1).

For the MIBP1 process also, we can write a closed set of coupled linear evolution equations for the average number of cells at site $\vec{R}$ at time t. But we need to define $2d$ variables at each site. Let $\bar{n}(\vec{R}, t, e_\alpha)$ denote the average number of cells residing at the site $\vec{R}$ at time t, whose mother cell is along the bond $\mathbf{e}_\alpha$. Here α takes $2d$ possible values $\pm 1, \pm 2, \ldots, \pm d$, and e_1 is the unit vector along coordinate x_1, and $e_{-1} = -e_1$. Then, the variables $\bar{n}(\vec{R}, t, e_\alpha)$ evolve according to the equations

$$\frac{d}{dt}\bar{n}(\vec{R}, t, e_\alpha) = \sum_{\alpha' \neq -\alpha} n(\vec{R} + e_\alpha, t, e_{\alpha'}) \tag{3.14}$$

Again, we define the Fourier transform variables of $\bar{n}(\vec{R}, t, e_\alpha)$ as $\tilde{n}(\vec{k}, t, e_\alpha)$ as

$$\tilde{n}(\vec{k}, t, e_\alpha) = \sum_{\vec{R}} \exp(i\vec{k}.\vec{R})\bar{n}(\vec{R}, t,_\alpha) \tag{3.15}$$

Then, the equations for different $\vec{k}$ decouple, and the infinite set coupled equations reduces to that of $2d$ coupled variables $\tilde{n}(\vec{k}, t, e_\alpha)$, for the $2d$ values of α for fixed $\vec{k}$. These are easily

seen to be

$$\frac{d}{dt}\tilde{n}(\vec{k},t,e_\alpha) = \exp(-ik_\alpha)\left[S(\vec{k}) - \tilde{n}(\vec{k},t,-e_\alpha)\right] \tag{3.16}$$

$$\frac{d}{dt}\tilde{n}(\vec{k},t,-e_\alpha) = \exp(ik_\alpha)\left[S(\vec{k}) - \tilde{n}(\vec{k},t,e_\alpha)\right] \tag{3.17}$$

where $\alpha = 1, 2..d$, and $S(\vec{k}) = \sum_{\beta=1}^{d}[f_\beta + f_{-\beta}]$. This may be written as

$$\frac{d}{dt}\tilde{n}(\vec{k},t,\alpha) = \sum_{\alpha'} M_{\alpha,\alpha'}(\vec{k})\ \tilde{n}(\vec{k},t,\alpha') \tag{3.18}$$

The eigenvalues for this $2d \times 2d$ matrix for a fixed $\vec{k}$-block are easily determined. For the eigenvalue λ, we define the eigenvector of the matrix be f_α. We discuss the diagonalization of the matrix M. Explicitly, the matrix elements are

$$M_{\alpha,\beta} = \exp(ik_\alpha), \quad \text{if} \beta \neq -\alpha; \tag{3.19}$$

$$= 0, \ \text{if} \alpha = -\beta. \tag{3.20}$$

Here the indices α and β take values $(\pm 1, \pm 2, \pm 3..\pm d)$ For the eigenvalue λ and its eigenvector f_α, we have, for $\alpha = 1$ to d

$$\lambda f_\alpha = e^{-ik_\alpha}[S(\vec{k}) - f_{-\alpha}] \tag{3.21}$$

$$\lambda f_{-\alpha} = e^{ik_\alpha}[S(\vec{k}) - f_\alpha] \tag{3.22}$$

where

$$S(\vec{k}) = \sum_{i=1}^{d} = [f_i + f_{-i}]. \tag{3.23}$$

We try to solve the coupled equations for f_α and $f_{-\alpha}$ in terms of $S(\vec{k})$. When $\lambda^2 \neq 1$, we can solve these equations to give

$$f_\alpha = \frac{e^{ik_\alpha}\lambda - 1}{\lambda^2 - 1} S(\vec{k}); f_{-\alpha} = \frac{e^{-ik_\alpha}\lambda - 1}{\lambda^2 - 1} S(\vec{k}) \tag{3.24}$$

Then, the consistency condition 3.23 becomes

$$\lambda^2 - 1 + 2d = 2\lambda\left[\sum_{i=1}^{d} \cos k_i\right] \tag{3.25}$$

This is a quadratic equation in λ, and has two roots. We denote the larger one by λ_{max}. this gives

$$\lambda_{max} = \Lambda + \sqrt{\Lambda^2 - 2d + 1}. \tag{3.26}$$

where we have defined $\Lambda = \sum_{i=1}^{d} \cos(k_i)$.
Writing $\vec{R} = \vec{u}t$ allows us to write

$$\bar{n}(\vec{u}t, t) = \int \frac{d\vec{k}}{(2\pi)^d} \exp\left[t\left(i\vec{k}.\vec{u} + \Lambda + \sqrt{\Lambda^2 - 2d + 1}\right)\right] \tag{3.27}$$

The above integral can be easily evaluated in the long time limit using the method of steepest descent giving

$$iu_j - \sin k_j \left[\frac{\sqrt{\Lambda^2 - 2d + 1} + \Lambda}{\sqrt{\Lambda^2 - 2d + 1}}\right] = 0 \tag{3.28}$$

The stationary point occurs at a imaginary value of $\vec{k} = i\vec{\kappa}$ which upon substitution gives

$$\kappa_j = \sinh^{-1} \frac{u_j}{\beta} \tag{3.29}$$

where

$$\beta = \frac{\sqrt{\Lambda^2 - 2d + 1} + \Lambda}{\sqrt{\Lambda^2 - 2d + 1}} \tag{3.30}$$

This gives us

$$\Lambda = \sum_{j=1}^{d} \sqrt{1 + (\frac{u_j}{\beta})^2} \tag{3.31}$$

Now we can write

$$\bar{n}(\vec{u}t, t) \sim \exp\left[t(\Lambda + \sqrt{\Lambda^2 - 2d + 1} - u_j \sinh^{-1} \frac{u_j}{\beta})\right] \tag{3.32}$$

Equation of the boundary is then obtained to be

$$\sum_{j=1}^{d} \Lambda + \sqrt{\Lambda^2 - 2d + 1} - u_j \sinh^{-1} \frac{u_j}{\beta} = 0 \tag{3.33}$$

Eq(3.30, 3.31 and 3.33) together form a set of coupled equations that give us the exact shape in the MIBP1.

3.5 Cluster shape in modified IBP$_2$

We now define another version of the IBP which is modified in the following way: we start with a single eve cell at the origin at $t = 0$, with the rest of the lattice empty. We break the time evolution of the process in time intervals of Δ. At time $z\Delta$ where z is real and non-negative, all cells at site $\overrightarrow{r}$ perform an IBP till time $(z+1)\Delta$ given the constraint that no descendants of any cell at $\overrightarrow{r}$ can give rise to daughter cells at $\overrightarrow{r}$. This modified evolution is captured by the modified propagator $G'(R, \Delta)$ given by

$$G'(\overrightarrow{R}, \Delta) = G_0(\overrightarrow{R}, \Delta) + [1 - G_0(0, \Delta)]\, \delta_{\overrightarrow{R},0} \tag{3.34}$$

In Fourier space,

$$\widetilde{G'}(\overrightarrow{k}, \Delta) = e^{2\Delta \sum \cos k_i} + 1 - I_0^d(2\Delta) \tag{3.35}$$

To evolve this system up to time t, it is immediately noted that the propagator needs to be applied iteratively and the result takes the form

$$\widetilde{G'}(\overrightarrow{k}, t) = \widetilde{G'}(\overrightarrow{k}, \Delta)^{t/\Delta} \tag{3.36}$$

Upon taking an inverse Fourier transform and substituting for $\overrightarrow{R} = \overrightarrow{u}t$, we get

$$G(\overrightarrow{u}t, t) = \frac{1}{(2\pi)^d} \int \overrightarrow{dk} e^{\left[t\left(\frac{1}{\Delta}\log\left(e^{2\Delta \sum \cos k_j} + 1 - I_0^d(2\Delta)\right) + i\overrightarrow{k}.\overrightarrow{u}\right)\right]} \tag{3.37}$$

The above integral can be easily evaluated in the long time limit using the method of steepest descent giving

$$iu_j + \frac{1}{\Delta} \frac{\left(e^{2\Delta \sum \cos k_i}(-2\Delta \sin k_j)\right)}{e^{2\Delta \sum \cos k_j} + 1 - I_0^d(2\Delta)} = 0 \tag{3.38}$$

The stationary point occurs at a imaginary value of $\vec{k} = i\vec{\kappa}$ which upon substitution gives

$$u_j = \frac{2}{\Gamma} \sinh \kappa_j \tag{3.39}$$

where

$$\Gamma = \frac{e^{2\Delta \sum \cosh \kappa_j} - I_0^d(2\Delta) + 1}{e^{2\Delta \sum \cosh \kappa_j}} \tag{3.40}$$

One can eliminate κ from the above equation using $\sinh^{-1} \frac{\Lambda}{2} u_j = \kappa_j$ which gives the equation

$$\ln(1-\Gamma) = \ln\left(I_0^d(2\Delta) - 1\right) - 2\Delta \sum_{j=1}^{d} \sqrt{1 + \left(\frac{\Gamma}{2} u_j\right)^2} \tag{3.41}$$

It is clear that if Δ is close to zero, then the capping is ineffective as for small Δ, evolution is effectively already capped. Also, for very large Δ, this method would be ineffective as only the origin would be capped and the evolution of the MIBP2 would be very much like the IBP. Hence, Δ can be optimized over and then, Eq(3.39-41) for a set of coupled equations whose solution gives the exact shape of the MIBP2 cluster.

3.6 Summary

We discussed bounds to the asymptotic shape of Eden clusters by first calculating the exact shape of the IBP cluster. We showed that even in the IBP cluster, a departure from the circular shape of cluster is seen as pointed out by Alm and Deijfen for the Eden cluster. Then we improved upon the bounds by considering two independent modifications to the IBP - one in which each cell independently gives rise to daughter cells at neighbouring sites except along the bond that connects it to its mother cell and the other, in which we iteratively evolve the system and in each iteration, impose the condition at a non-empty site, no more cells can be added due to the descendants of the cells present at that site.

Can we write an equation for $\bar{n}(\vec{R}, t)$ when the process is not Markovian?

Definition of the non-Markovian model: We consider an infection process on $\mathbf{Z^2}$ in which the number of cells present at a site can be arbitrarily large. At the time $t = 0$, there is only one cell present in the system, and it is placed at the origin $\vec{O}$. At any time $t > 0$, a cell can give birth to a daughter cell, that sits at a nearest neighbor site. Then the number of cells at the neighbor increases by one. Once born, a cell never dies. We assume that a cell gives birth to a daughter cell independently along each bond, independent of the number of cells present at the site, or at neighbours. The random time after which a cell gives birth along a particular bond follows a distribution $G(t)$ (not exponential).

This process is more complicated than the Markovian IBP because, in this process, when a cell gives rise to a daughter cell along one bond, the clocks on other bonds connected to it continue to age. In the Markovian case, one could assume that all the clocks reset when a birth event happens.

Suppose the process was not on a lattice and we are only interested in studying the size of the growing population (starting from a single cell), it is easy to see that the average total number of cells at time t will be given by:

$$\bar{n}(t) = 1 + \int_0^t \bar{n}(t-u) d\bar{N}(u)$$

where $d\bar{N}(u)$ represents the average number of births in the time interval $[u, u + du]$ and $\bar{n}(t - u)$ represents the average total number of their children up to time t .

One can do slightly better by assigning weights to different Galton-Watson trees and through this, get information about the number of cells in each generation at any given time. However, to tackle the problem of spatial distribution of cells on the lattice, the Montroll-Weiss like approach seems most promising. Let $Prob(n, R, t)$ be the probability that there are n cells at site R at time t. We can write:

$$Prob(n, R, t) = \sum_{N=0}^{\infty} Prob_t(N) Prob_R(n)$$

where $Prob_t(N)$ denotes the probability of observing N total births up to time t and $Prob_R(n)$ is the probability that n out the N births happened at site R.

Answering this will allow us to extend the analytical methods developed in this chapter for the Eden process to a First Passage Percolation problem with arbitrary passage time distributions.

Chapter 4

Chase-Escape Percolation

In the last chapter we studied a simple stochastic model for how fast a rumor can spread starting from a single source. But what if the spreading of a rumor is accompanied by a competing process of scotching this rumor? Is it possible that the rumor continues to spread even if it is being spread at a significantly slower rate than the rate of scotching the rumor? In the model *Chase-Escape* percolation, which is the main focus of this chapter, the answer is *Yes.* This model displays an intriguing phase transition for the spreading of rumor but more interestingly, the critical point for this phase transition appears to be the same as that of bond percolation − a classic problem in percolation theory. Could it be that this mysterious is actually bond percolation in disguise? Here, we try to address this question along with studying the process above and below criticality as well.

4.1 Introduction

Studying the dynamics of interacting populations is a fundamental problem in Biology. However, mathematical models that are inspired by such dynamics often become problems of great interest in Statistical Physics as they display rich and interesting features. In this work, we study a prey-predator model, called *Chase-Escape percolation* [34, 37], on a lattice in which, coexistence between prey and predator is possible even when the prey is moving significantly slower than the predators.

Chase-Escape (CE) percolation on hypercubical lattices can be defined as follows: Consider a process on a $d-$dimensional hypercubical lattice where each site can either be occupied by a blue species particle (predator), a red species particle (prey) or it can remain vacant. We denote the coordinates of each site by $(x_1, x_2, ..., x_d)$. At time $t = 0$, origin O=$(0, 0, ..., 0)$ is occupied by a blue particle, a neighbour of the origin, O'=$(1, 0, ..., 0)$ is occupied by a red particle and all other sites are vacant. The evolution is a continuous time Markov process in which a red particle can give birth to another red particle at a vacant neighbouring site at rate p and a blue particle can eat up a red particle at a neighbouring site at rate 1. When a blue particle eats up the red particle on a neighbouring site, that site is then occupied by another blue particle. As defined, in this model, preys can only create copies of themselves at neighbouring vacant sites and predators can only create copies of themselves at a nearest neighbour site occupied by a prey that it can eat.

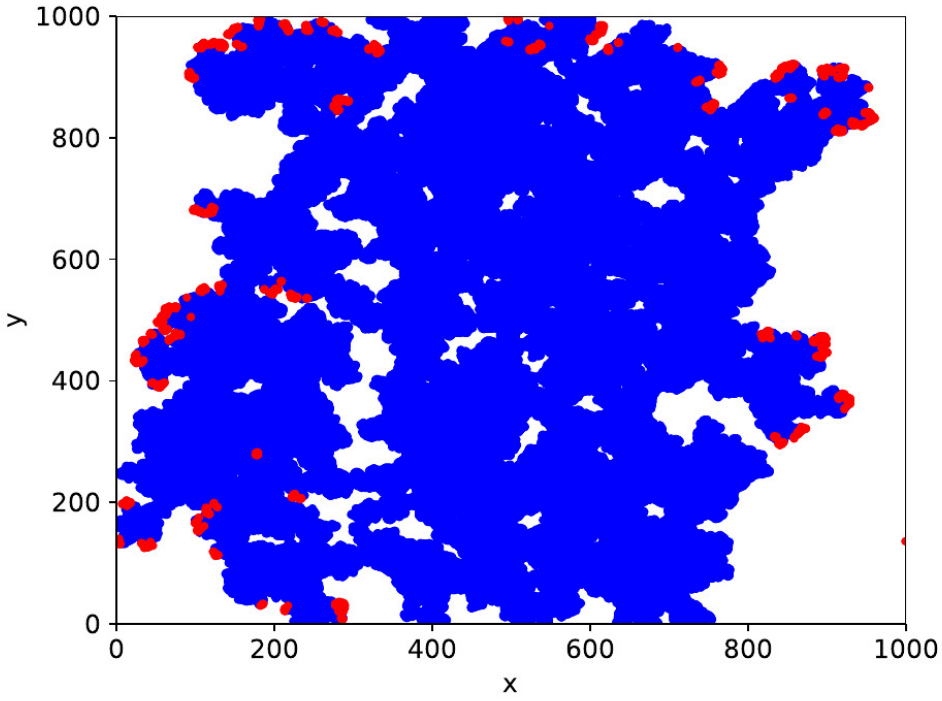

Figure 4.1: A realization of the Chase-Escape process just above the critical point on a 1000x1000 square lattice.

This model has been studied on $k-$ary trees [34] with initial conditions such that the predator is located at the root and the prey occupy the k daughters of the root. It was

shown that the critical value for coexistence in this case is given by

$$p_c(k) = 2k - 1 - 2\sqrt{k^2 - k}$$

which in large k limit gives

$$p_c \sim \frac{1}{4k}$$

It was later proved that survival probability is non-zero only if p is strictly greater than p_c. Clearly, it is seen that the prey can survive on such trees even if it moves at a slower rate than the predators. It is also noted that the critical value p_c goes down as k increases. This is expected as increase in k denotes the increase in the number of ways prey can escape. This problem was also studied on the ladder graph and it was found that its critical value is 1. But what about the behavior on the $2D$ square lattice?

4.2 Improved determination of critical survival probability p_c

Numerical studies [35] showed conclusively that even on the square lattice, coexistence between the prey and predator is possible when the rate of spreading of prey p is strictly less than that of the predator. This is expected as the effective rate of spreading of predators depend on the number of prey and when the number of prey decrease, the predator slows down, allowing for the prey population to replenish in numbers. But more strikingly, it was shown through simulations that the critical value for the survival of prey is $p_c \approx 0.5$. However, what is striking is the critical value of 0.5 which is equal to the critical value for the bond percolation problem on the square lattice [35]. Could it be that Chase-Escape percolation is just bond percolation in disguise? To investigate this question, we use numerical methods to determine the critical value accurately up to three decimal places. We simulated the process on $L \times L$ lattice with periodic boundary conditions along the $y-$axis and initial conditions such that each site on the line $x = 0$ is occupied by a blue particle and each site on the line $x = 1$ is occupied by a red particle. It is well known that this initial condition with a line of particles is better behaved as it has a self-averaging property and shows a sharper transition than the initial condition where we start with a single prey and predator. Throughout this chapter, we will work the initial conditions where we start with a line of prey adjacent to a

line of predators. These two lines can be thought of as two competing surfaces. Extinction occurs when the surface of prey is eaten up by the predator surface. In such a situation, the system goes into one of its many absorbing states.

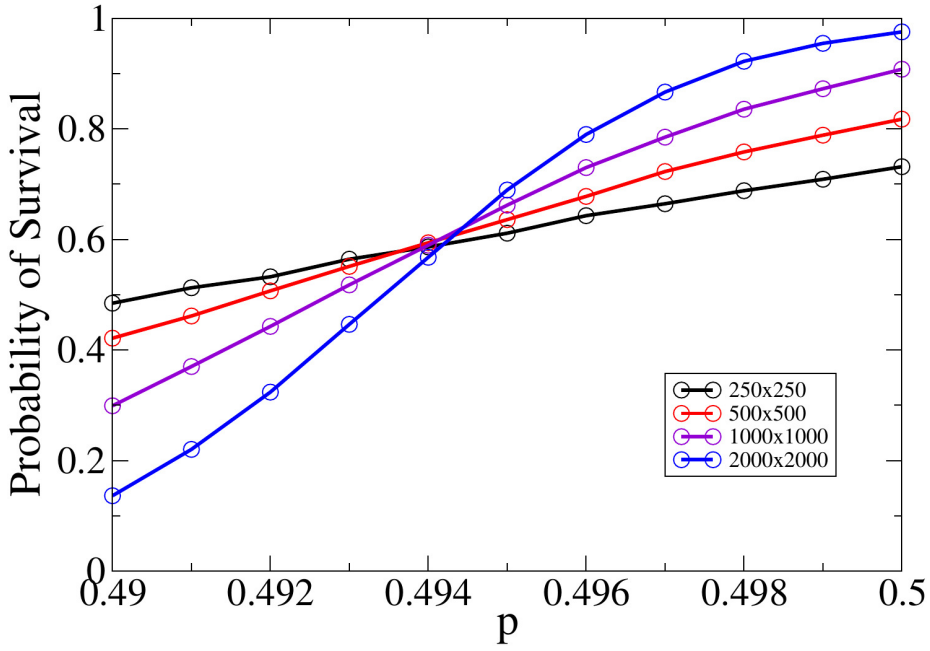

Figure 4.2: Survival probability as a function of p is plotted for lattice sizes $L = 250, 500, 1000$ and 2000. Observe the coincidence of curves away from $p = 0.5$. The critical probability is determined to be 0.4943 ± 0.001

For simulation purposes, we work on finite lattices and see how the survival probability scales as a function of the lattice size. In a simulation, the prey is said to survive if any of the prey particles are able to reach the line $x = L$ starting from the line $x = 1$ as defined in the initial condition. Survival probability is then calculated by doing the simulation multiple times and computing the fraction of realizations in which the prey survives. We find that the critical probability for the survival of red species is 0.4943 ± 0.001. The plot can be seen in Figure 4.2 where the simulation has been done on lattice sizes $L = 250, 500, 1000$ and 2000 and the probability of survival is calculated by doing a configuration averaging over 50000 realizations. This provides strong evidence against the idea that Chase-Escape might be a bond percolation in any trivial way.

In Figure 4.3 we demonstrate the scaling collapse of survival probability curves for different lattice sizes. We obtain a good data collapse at the value $p_c = 0.4943$ and $\nu = 1.33$. The critical exponent thus obtained is consistent with the standard $2-$D percolation universality

class. This encourages one to draw parallels with the SIR model on a square lattice which belongs to the same universality class. In the SIR model, in an outbreak, each site is either Susceptible, Infected or Recovered. Infected sites can infect neighbouring sites that are susceptible and each infected site can recover indepently. In some variants of this process, recovered sites become susceptible again with added immunity. In CE percolation, the vacant sites can be thought of as susceptible, red sites as infected and blue as recovered. The key difference between the two models however is that in the SIR process, the recovery of each infected particle is independent of others whereas in CE, there are nontrivial correlations owing to the fact that the blue particles always form a connected cluster.

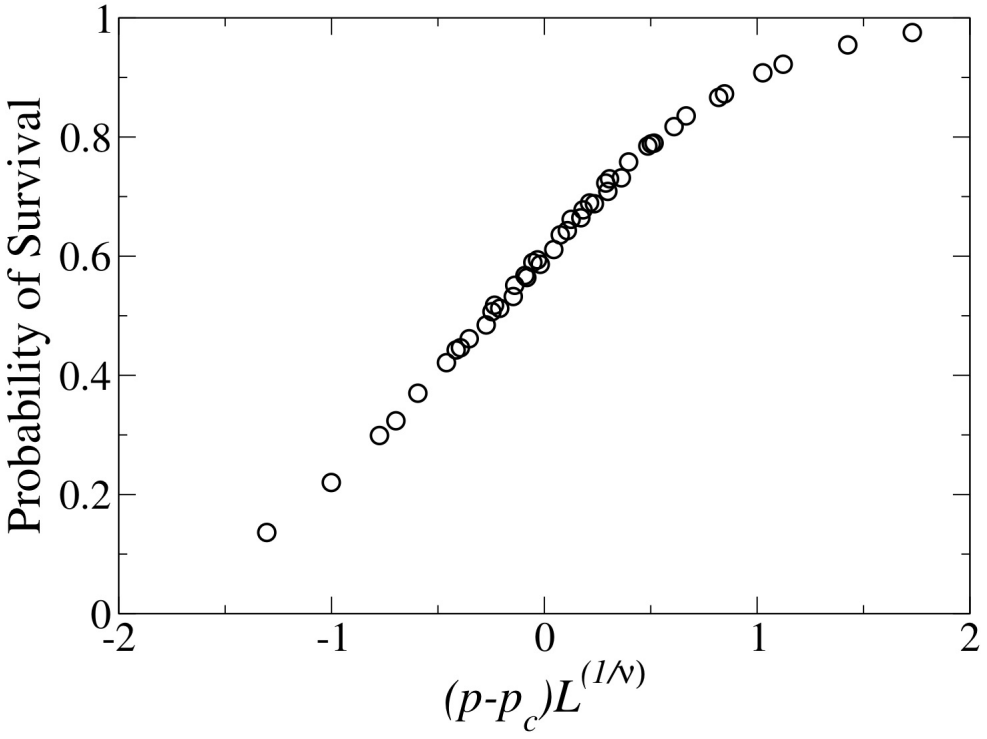

Figure 4.3: Scaling collapse for the survival probability at $\nu = 1.33$ and $p_c = 0.4943$. $\nu = 1.33$ is the value of the standard $2-$D percolation universality class.

4.3 p_c in the diagonal direction

In Chapter 3, we studied the asymptotic shape of growing Eden clusters. One striking feature about the shape of Eden clusters is its departure from the circular shape. It was shown in Alm and Deijfen that even in $2-$D, there is a significant difference in the velocity of the

front along the axis and along the diagonal direction. Taking inspiration from this, a natural question to ask is: Is the value of p_c different along different directions? We investigated the critical behaviour of CE in the diagonal direction by initializing a modified line initial condition on the square lattice tilted by 45 degrees as shown in Figure 4.4. We find that the critical rate is still 0.4943 ± 0.001 which is the same as the critical value along the axis, as seen in Figure 4.5. However, there is a clear increase in the survival probability when compared with the survival probability along the axes. This is expected as the red particles have more sites to escape to along the diagonal (can be seen in Figure 4.4).

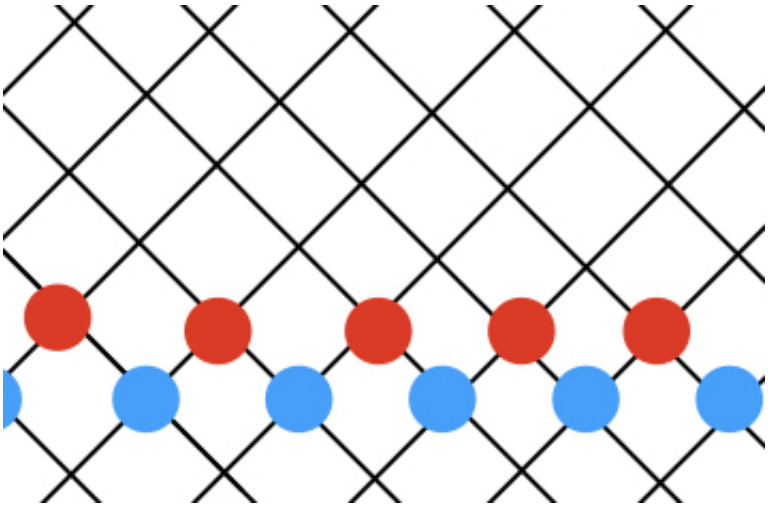

Figure 4.4: A schematic of the initial conditions used to investigate the critical behavior of CE along the diagonal direction in the $2-$D square lattice.

This motivates an attempt at writing down a master equation for the Chase-Escape process on the $D-$dimensional hypercubical lattice along the major direction $(1, 1, ..., 1)$.

4.3.1 Chase-Escape along the major diagonal direction: An ad-hoc approximation

Consider the propagation of red sites in the $(1, 1, ..., 1)$ direction in $D-$dimensions. Then, near the front, we have the approximate equation:

$$\frac{dn(t, R)}{dt} = pDn(t, R-1) - n(t, R)$$

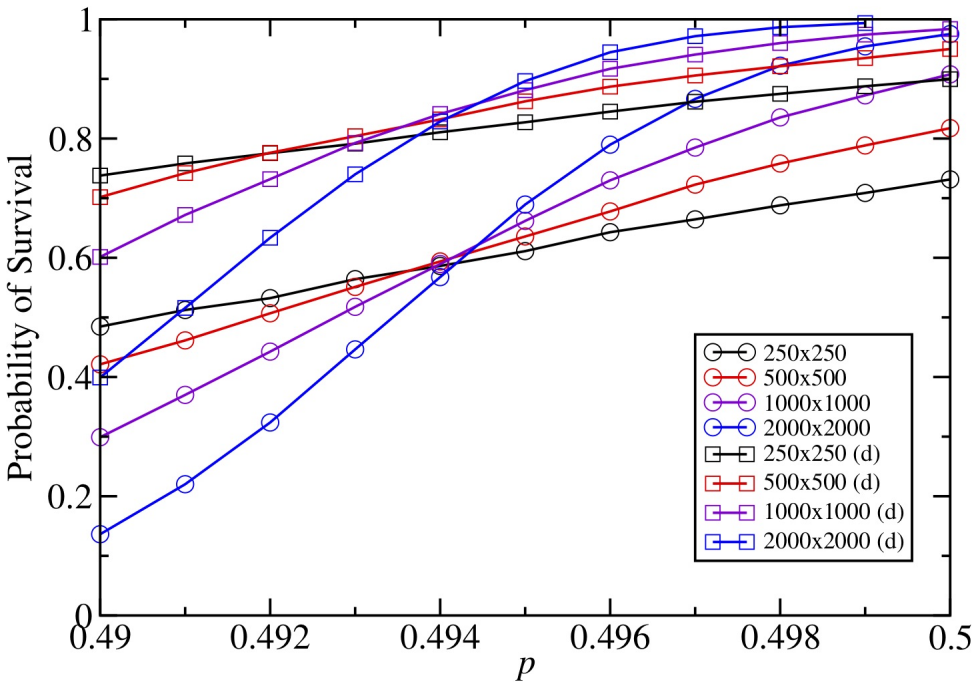

Figure 4.5: The critical probability calculated along the axial and the diagonal direction is determined to be 0.4943 ± 0.001. However, the survival probability along the diagonal direction is significantly higher − which is expected as the red particles have more sites to escape to along the diagonal.

where R labels the hyperplane along the major diagonal direction containing the point $(R, R, ..., R)$ and $n(t, R)$ is the total number of red sites on that hyperplane at time t. Here, the first term on the right hand is the contribution of red site on the hyperplane $(R-1)$ to $n(t, R)$ as each red site on hyperplane $(R-1)$ would have D forward neighbors at R and each will infect a site at R at rate p. We assume that we may ignore the probability that a site at R is already infected. The second term indicates the rate at which red on the hyperplane R are eaten up by blue on $(R-1)$. We assume that each has red on R has one backward blue neighbor.

We make a change of variables to $n(t, R)e^t = f(t, R)$ and we get

$$\frac{df(t, R)}{dt} = f(t, R-1)$$

which admits the solution

$$n(t) \sim (pDt)^R e^{-t}/R!$$

which has the form of a travelling wave and in $D = 2$, it gives $p_c = 1/2$.

While there are many simplifying assumptions in this modeling, it is able to capture the basic phenomenology of Chase-Escape.

4.4 Dynamics of the front: The depinning transition

If we define the CE model as a problem with two interacting surfaces, many questions arise naturally. But one important question that we choose to address here is: What does the dynamics of the CE front look like at $p_c < p < 1$. We will first define what we mean by front in this context. On the lattice, starting from the line initial condition as defined above, it is clear that both the interacting surfaces are going to spread rightward. We define the front as the set of the sites that have the largest $x-$coordinate for each $y-$coordinate among all sites. It is easy to see that the front separates the cluster of occupied sites from the vacant sites. We define the red front as the subset of sites from the front that are red. Similarly, we define a blue front. The quantity of interest for us in this analysis is going to be the $x-$coordinate of the centre of mass of the red and blue fronts (X_{avg}). For $p > 1$, the width between the red and the blue fronts will increase linearly with time. For $p < p_c$, the system goes into one of its absorbing states and the front has no dynamics asymptotically.
The simulations in this section have been done on a lattice of dimensions 500×5000 with periodic boundary conditions along the $y-$axis. For $p_c < p < 1$, interestingly, the centre of mass of the blue sites and the red sites on the front coincide at all times. In this regime, the two fronts are *pinned* together and at $p = 1$, a *depinning transition* happens. Clearly, in Figure 4.6, we see that the blue and the red front move together. More interestingly, the CE front on an average travels slower than the Eden front moving at rate p. This is quite a counter-intuitive result as one would expect that the surviving red are completely unaffected by the blue predators and hence would continue to travel at the Eden speed. Figure 4.7 is a plot of CE and Eden fronts at values $p = 0.6, 0.8$ and 1. We can see that the Eden and CE fronts coincide at $p = 1$. However, at $p = 0.6$, the CE front travels significantly slower. In the inset of Fig.4.6, the dashed green line is the velocity of Eden front as obtained by Alm and Deijfen [26]. Our simulation of the Eden front is in agreement with their result while the CE front clearly lags behind. The inset of Fig.4.7 reveals that the velocity of the CE front in the pinned regime is not linear in p.

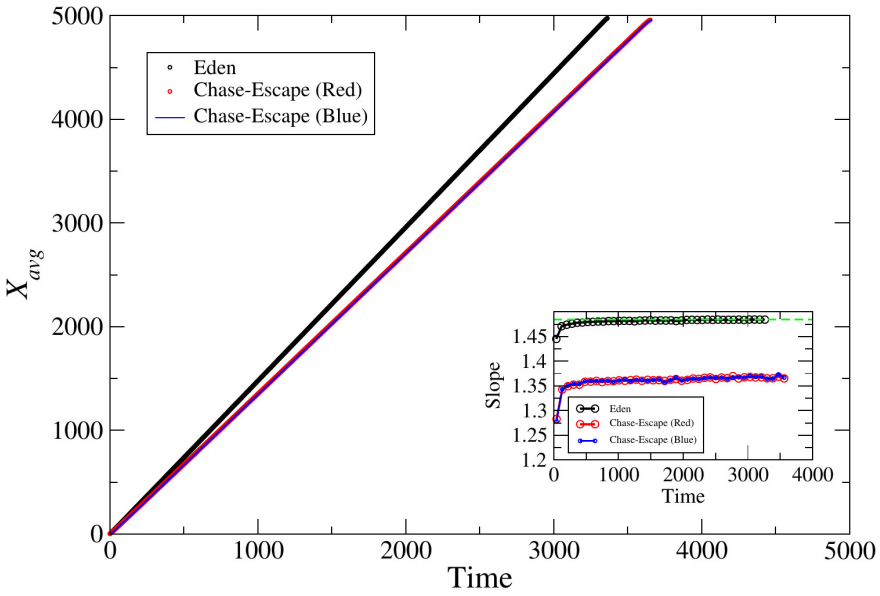

Figure 4.6: Dynamics of the Chase-Escape and Eden fronts at $p = 0.6$. It is easily seen that the centre of mass of the blue sites and the red sites on the front coincide at all times showing that in the regime $p_c < p < 1$, the red and blue fronts are *pinned* together. Observe that at $p = 0.6$, the Chase-Escape front travel significantly slower than the Eden front. Inset is a plot of velocity as a function of time to check for convergence of velocity. We plot this by discretizing the calculation of slope and plot it as a function of time. Slope is given by: $(X_{avg}(t + 100) - X_{avg}(t))/100$.

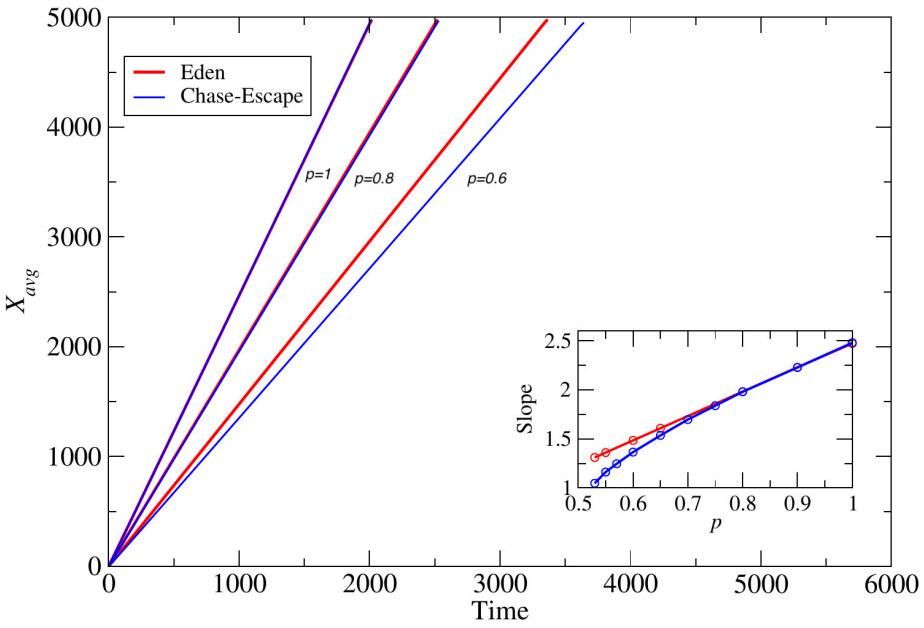

Figure 4.7: Chase-escape and Eden fronts at values $p = 0.6, 0.8$ and 1. We can see that the Eden and red CE fronts coincide at $p = 1$. As pointed in Fig.4.6, the red CE front is significantly slower than the Eden front at $p = 0.5$. Inset is a plot of velocity of the CE and Eden fronts as a function of p. Clearly, velocity of the CE front in the pinned regime is not linear in p.

What can be the possible mechanisms that can lead to the slowing down of the front? A clear diiference between the CE and Eden front is that the CE front consists of immobile parts (blue sites) that can only move when there is a red site in front of it. However, if we only look at the speed of the centre of mass of red CE front, it may be expected that this front should behave just like the centre of mass Eden front. The argument is as follows: The surviving red sites on the front are the ones who have not been eaten up by the blue and hence, have not felt the presence of predation. This phenomenon is in fact common in many prey-predator models of biology. However this does not seem to be the case in the CE model which points towards the fact that, the presence of predation is felt by the surviving prey on the front too. However, the only way the predator can have made an impact on the surviving prey is by limiting the area in which they can spread. In CE, it seems like this factor is dominant but we require further analysis to verify this. One another possible mechanism for slowing down the CE front could be that often times, the farthest red is getting eaten up and then the maximum position of the front, defined as largest x coordinate of a surviving red particle is set back and then starts increasing again. This is plausible as the blue front is

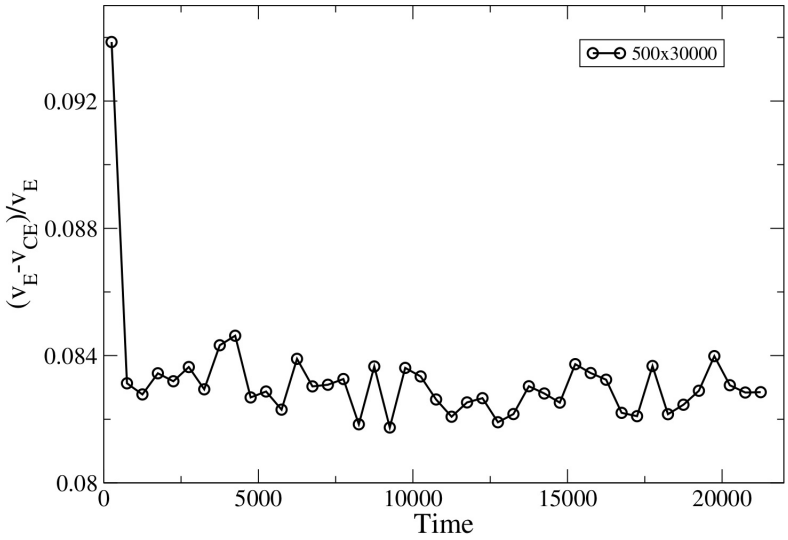

Figure 4.8: Relative difference between the velocities of the Eden and CE plotted as a function of time at $p = 0.6$. This simulation has been done on a lattice of size 500×30000 to rule out slow convergence of the speed of red CE front to the Eden front. It is evident that there is no systematic approach to zero.

always pinned to the red front. There very well might be some red sites that by chance move forward quickly. However, when the blue sees this stretch of red sites, it catches up very fast naturally (because it is travelling faster) and slows down only near the front where red sites are less. The same slowing down happens when the blue catches up with red sites which were travelling at a slightly slower speed than the fast ones. Hence, the killing of red sites on the front happens to the leaders also at a finite, though smaller rate and this contributes to the chase-escape front velocity being less than the Eden front velocity. Fig.4.9 shows why this argument might be true. Two trajectories of the maximum extent of infection at $p = 0.6$ for Eden front and the red front in CE are plotted. Inset shows a zoomed in picture of the trajectory of the CE front where it is clearly visible that the maximum position of a red infection does drop quite often. Fig.4.10 shows four other instances from the trajectory of the maximum red front where the drop is clearly visible.

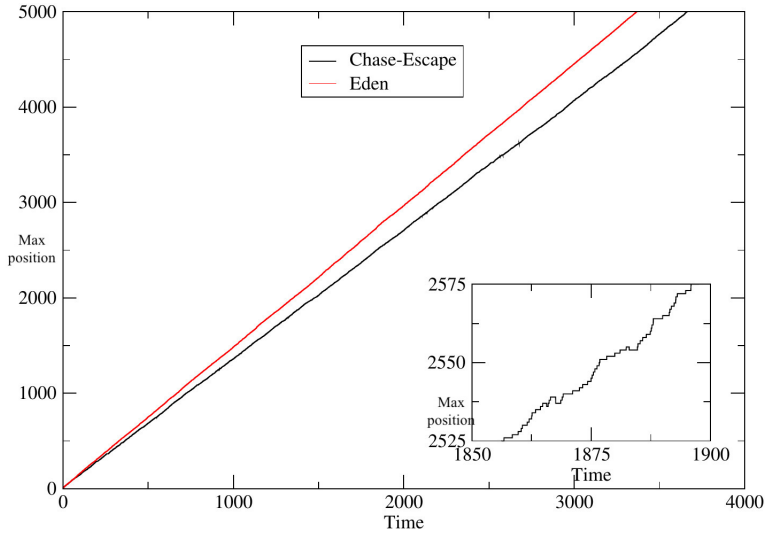

Figure 4.9: Two trajectories of the maximum extent of infection at $p = 0.6$ for Eden front and the red front in CE are plotted. Inset shows a zoomed in picture of the trajectory of the CE front where it is clearly visible that the maximum position of a red infection does drop quite often.

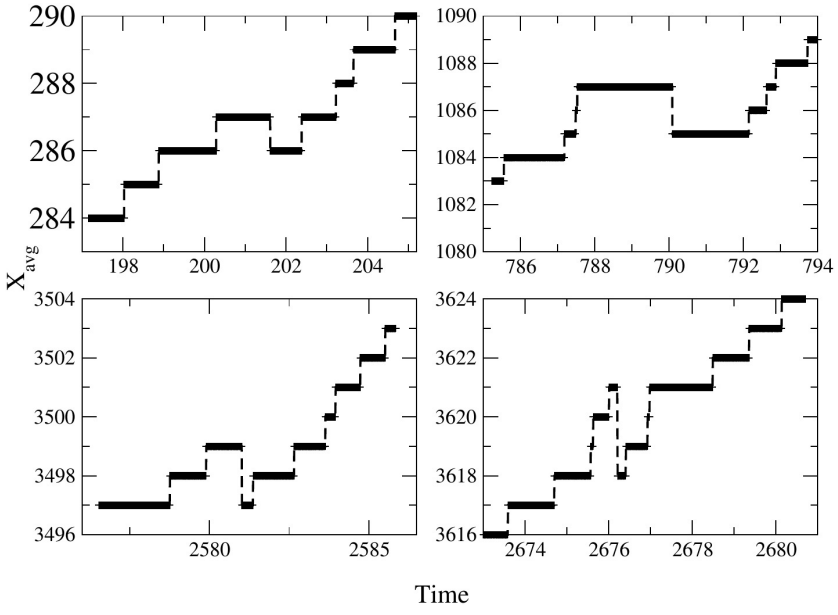

Figure 4.10: Four instances from the trajectory in Fig.4.9 where there is a drop in the maximum position of the red front.

4.5 Lower bound to the cluster size in the absorbing state

So far, our analysis was focused on properties of this process at p_c and above it. In this section, we shift the focus of the discussion to $p < p_c$. Consider the Chase Escape percolation on the $d-$dimensional hypercubical lattice starting from the initial condition that the origin O is occupied by a red species particle and a blue species particle is present at a site Q which is connected to O with an edge but is not part of the lattice. This choice of initial condition is chosen for convenience in calculations. We look at values of $p < p_c$. It is clear that in this case, the system finally goes into one of its absorbing states and we are left with a cluster of blue sites. We are interested in knowing the distribution of the sizes of these clusters. If we look at the probability that, in the absorbing state, there are more than s number of blue particle and call it $Prob(B > s)$, the we immediatiely have

$$Prob(B > s) \geq C_1 \exp\left[-\frac{C_2 s^{1/d}}{p}\right] \tag{4.1}$$

where C_2 and C_2 are constants independent of p. The idea behind this bound is the fact that $Prob(B > s)$ is bounded from below by the probability that by the time blue creates a copy of itself for the first time, red species has already created s copies of itself. The probability that the blue does not give birth until time T is just $\exp[-T]$. And in time T, the number of red particles is of order $(pT)^d$.

Since $Prob(B > s)$ is bounded from below by a stretched exponential function, it is clear that $Prob(B > s)$ cannot decay as an exponential in s. This in contrast to ordinary percolation, where for values below the critical threshold, the cluster size distribution follows an exponential decay [22, 36].

4.6 Summary

In summary, we studied the Chase-Escape percolation on the $2-$D square lattice at determined its critical value using numerical simulations to be $p_c = 0.4943 \pm 0.001$ amd we found scaling collapse with exponent $\nu = 1.33$, the standadrd value for undirected prcolation in 2d.

This provides strong evidence against the idea that Chase-Escape percolation might be the bond percolation in disguise. We also established that the critical behaviour of this process in different directions is not different by finding that $p_c = 0.4943 \pm 0.001$ in the diagonal direction as well. Apart from this phase transition, the Chase-Escape front also undergoes a *depinning* transition. For $p_c < p < 1$, the center of mass of the red and blue fronts coincide as a function of time and the two fronts move together in a *pinned* way. However, interestingly, we found that the speed of the Chase-Escape front is smaller than the speed of the Eden front for the same value of p. Using simulations, we provided a possible mechanism for this counter-intuitive phenomena. Finally, we studied the problem for $p < p_c$ and obtained a stretched exponential lower bound to the distribution of cluster sizes. However, our understanding of the problem is still far from complete; there are several open directions left to be explored. Most importantly, can it be proved that survival for $p < 1$ is a possibility on the 2D square lattice? A new set of opportunities open up if we introduce a third species into this problem that can spread on to only blue sites. Moreover, if we allow for cyclic interactions where the red can also spread on to the new species, many new and interesting features are expected to emerge.

Chapter 5

Summary and Future Directions

We are now moving close to the end of this journey. But no journey is complete until we take a moment to look back and reflect upon the little steps that have made it worthwhile. In this chapter, we will briefly recall the main results obtained in this thesis and discuss a few interesting directions that these results give rise to and which might be worth pursuing as another journey sometime in the future.

In this thesis, we studied stochastic processes that have made their way into Statistical Physics as models of out-of-equilibrium phenomena. We mainly focused on three models: a two-species exclusion process, Eden model and Chase-Escape percolation. While these models have generated interest amongst statistical physicists, all three of them have been motivated by problems in Biology. We started off by studying the two-species exclusion in which the second class particle showed a remarkable phenomena, called the *TASEP Speed Process*, where even after the system's evolution was Markovian, its late time dynamics was strongly dependent on its initial dynamics. We provided a simple explanation for this intriguing phenomena by using an *effective medium* approach and modeling the motion of the second class particle as a random walk in a space-time dependent background field determined by the motion of the other particles in the system. We demonstrated how this approach could be extended to other more complicated problems and in the end of Chapter 2, discussed an interesting variation of the multispecies exclusion problem where the rate of exchange between adjacent particles depended on the difference between their class numbers. Even in this problem, the late time dynamics shows heavy dependence on

early time dynamics. While we have made some progress in explaining this phenomena too, there are still many open directions that can be pursued. In Chapter 3, we motivated the problem of cluster growth and why it is important to calculate bounds to the extent of growth. After convincing the reader that finding these bounds are important, we discussed how to calculate upper bounds to the shape of Eden clusters by first calculating the exact shape of the IBP cluster and two of its variants. We showed that even in the simplest IBP cluster, a departure from the circular shape of cluster is seen as pointed out by Alm and Deijfen for the Eden cluster. We then outlined an open problem whose answer can extend our analytical method to find bounds to the shape of clusters in the more general problem of First Passage Percolation, with arbitrary passage times. Finally, for the Chase-Escape problem in Chapter 4, using numerical simulations, we refuted the idea that $p_c = 0.5$ by accurately determining p_c up to three decimal places and showed that this critical value doesn't have a visible dependence on the direction in which we choose to study the growth. We further pointed out that apart from the extinction-coexistence transition, the model also undergoes a *depinning* transition at $p = 1$ where for $p_c < p < 1$ the centre of mass for the red and blue particles on the front move together and the two surfaces are *pinned*. We conclusively established a counter-intuitive result that for $p_c < p < 1$, the CE front travels slower than that of the Eden front and provided a possible mechanism for such a behavior. Finally, we provided a lower bound to the cluster size distribution at $p < p_c$. Several challenges still remain in this problem and our understanding of this process is far from being complete. Most importantly, can it be proved that survival for $p < 1$ is a possibility on the 2D square lattice? We provided an approximate phenomenological description to support this claim. However, many simplifying assumptions were made in that regard which weren't completely justified. Another interesting direction would be to see the effects of a third species introduced into the system. Taking inspiration from many real biological phenomena - including antibiotic resistance and production in E.Coli to mating strategies in male side-blotched lizard, we can include cyclic interaction among the different species. Many novel interesting features are expected to arise in such a process.

Bibliography

[1] K. Mallick, Physica A: Statistical Mechanics and Its Applications 418, 17 (2015).

[2] D. Chowdhury, L. Santen, and A. Schadschneider, Physics Reports 329, 199 (2000).

[3] O. Bnichou, P. Illien, G. Oshanin, A. Sarracino, and R. Voituriez, Journal of Physics: Condensed Matter 30, 443001 (2018).

[4] T. Chou, K. Mallick, and R. K. P. Zia, Reports on Progress in Physics 74, 116601 (2011).

[5] P. L. Krapivsky, S. Redner, and E. Ben-Naim, A Kinetic View of Statistical Physics (Cambridge University Press, 2010).

[6] S. Das, D. Dhar, and S. Sabhapandit, Physical Review E 98, (2018).

[7] V. Karimipour, EPL 47, 304 (1999).

[8] V. Karimipour, Phys. Rev. E 59, 205 (1999).

[9] N. G. V. Kampen, Stochastic Processes in Physics and Chemistry (Elsevier, 1992).

[10] B. Duplantier, in Einstein, 1905–2005: Poincar Seminar 2005, edited by T. Damour, O. Darrigol, B. Duplantier, and V. Rivasseau (Birkhuser Basel, Basel, 2006), pp. 201–293

[11] P. Echenique and J. L. Alonso, Molecular Physics 105, 3057 (2007).

[12] M. Schwartz and E. Katzav, J. Stat. Mech. 2008, P04023 (2008).

[13] F. Pegoraro, F. Califano, G. Manfredi, and P. J. Morrison, Eur. Phys. J. D 69, 68 (2015).

[14] P. A. Ferrari and C. Kipnis, Annales de l'I.H.P. Probabilits et Statistiques 31, 143 (1995).

[15] R. Livi and P. Politi, Cambridge Core (2017).

[16] G. Amir, O. Angel, and B. Valk, Ann. Probab. 39, 1205 (2011).

[17] H. Rost, Z. Wahrscheinlichkeitstheorie Verw Gebiete 58, 41 (1981).

[18] S. N. Majumdar and M. Barma, Phys. Rev. B 44, 5306 (1991).

[19] P. A. Ferrari, Probab. Th. Rel. Fields 91, 81 (1992).

[20] B. Derrida, S. A. Janowsky, J. L. Lebowitz, and E. R. Speer, J Stat Phys 73, 813 (1993).

[21] O. Angel, A. Holroyd, and D. Romik, Ann. Probab. 37, 1970 (2009).

[22] D. Stauffer, Physics Reports 54, 1 (1979).

[23] R. J. Allen and B. Waclaw, Reports on Progress in Physics 82, 016601 (2019).

[24] Q. Bertrand and J. Pertinand, Physics Letters A 382, 761 (2018).

[25] A. Auffinger, M. Damron, and J. Hanson, 50 Years of First-Passage Percolation (American Mathematical Soc., 2017).

[26] S. E. Alm and M. Deijfen, J Stat Phys 161, 657 (2015).

[27] H. Kesten, in From Classical to Modern Probability: CIMPA Summer School 2001, edited by P. Picco and J. San Martin (Birkhuser Basel, Basel, 2003), pp. 93 143.

[28] D. Dhar, Physics Letters A 130, 308 (1988).

[29] M. Kardar, G. Parisi, and Y.-C. Zhang, Physical Review Letters 56, 889 (1986).

[30] D. Dhar, in On Growth and Form: Fractal and Non-Fractal Patterns in Physics, edited by H. E. Stanley and N. Ostrowsky (Springer Netherlands, Dordrecht, 1986), 288 - 292.

[31] T. Williams and R. Bjerknes, Nature 236, 19 (1972).

[32] M. Eden, in (The Regents of the University of California, 1961).

[33] C. Bordenave, Electronic Journal of Probability 19, 1 (2014).

[34] S. Tang, G. Kordzakhia, and S. P. Lalley, ArXiv:1807.08387(2018).

[35] H. Kesten, Comm. Math. Phys. 74, 41 (1980).

[36] M. Aizenman and C. M. Newman, J Stat Phys 36, 107 (1984).

[37] R. Durrett, M. Junge, and S. Tang, ArXiv:1807.05594 (2018).